

# Analogues of eigenvectors and their control in nonautonomous finite-time flows

Sanjeeva Balasuriya

School of Mathematical Sciences, University of Adelaide, SA 5005, Australia

Under consideration for publication in *Journal of Nonlinear Science*, December 2015

## Abstract

In autonomous flows, eigenvectors of saddle fixed points are locally tangent to stable and unstable manifolds, which form important flow separators. Computing instantaneous eigenvectors however does not identify local flow separators in nonautonomous flows. This article characterises the correct analogue of eigenvectors, defined as local tangents to time-varying stable and unstable manifolds, in terms of a time-history of local velocity shear under a nearly nonautonomous ansatz. With microfluidic flow control in mind, a methodology for manipulating these directions in any prescribed time-varying fashion by applying a local velocity shear is developed. Availability of data for both infinite and finite time-intervals is considered. The results are verified for both smoothly and discontinuously time-varying directions using finite-time Lyapunov exponent fields, and excellent agreement is obtained.

## 1 Introduction

Transport in nonautonomous (unsteady) flows such as in oceanic and atmospheric jets and eddies/vortices/rings, or microfluidic channels with several fluids, is well-known to be strongly influenced by dominant flow structures and separators. Examples include the invisible flow barrier off the west coast of Florida which protected the coast during the Deepwater Horizon oil spill, the Antarctic polar vortex, and the interface between a microdroplet and a carrier fluid in a microchannel. These structures all move with time, and the ability to demarcate, manipulate, or control the flow across, such structures has profound implications at a range of scales from the geo-

physical to the nanofluidic. Over the last decade or two, the connection between such flow barriers and the dynamical systems concepts of stable and unstable manifolds has become well-established [48, 45, 67, 66, 9]. The results of this article are motivated by the desire to control these flow separators in a way that one chooses, with the idea of being able to govern the transport occurring in microfluidic devices. The fact that the flow is of low Reynolds number at microscales means that fluid mixing is suppressed; yet in many devices the wish is to improve mixing. By manipulating the flow separators, i.e., the stable and unstable manifolds, one can focus directly on the transport templates which regulate fluid mixing.

In autonomous (steady) flows defined for infinite times, the concepts of saddle-like fixed points and their eigenvalues and eigenvectors enable the determination of stable and unstable manifolds locally. The *global* structure of these invariant manifolds form a template which governs transport in space, yet their *local* structure (and indeed global definitions in terms of exponential decays) are associated directly with the eigenvalues and eigenvectors. In particular, the directions in which these emanate locally from the saddle point are defined by the eigenvectors. Unfortunately, in *nonautonomous* flows defined only for *finite* times—i.e., for any realistic situation based for example on observational or experimental data—*instantaneously computed* fixed points, eigenvalues or eigenvectors have no relevance to transport.

There are a variety of diagnostic techniques which purportedly identify transport templates in nonautonomous flows which are defined over finite times. There are variously defined as entities of extremal attraction/repulsion [31, 20, 74], minimal instantaneous flux/deformation [48, 12], extremal curve/surface length/area deformation [44, 46] or extremal curvature deformation [55], or ridges extracted from finite-time Lyapunov exponent (FTLE) fields [66, 67, 26, 40, 71, 51, 52, 22] or transfer (Perron-Frobenius) operator singular vector fields [36, 33, 37, 35]. Alternative methods identify these using topological braid theory [2], ergodic theory [23] or various averages along trajectories [68, 57, 56, 58]. Each of these diverse methods offer computational tools for extracting precisely its own definition; there are few theoretically established connections between them [45]. The *hyperbolic*-type transport templates are the generalisations of stable and unstable manifolds, and have strong theoretical connections to exponential dichotomies [27, 65, 16] and the Oseledets splitting [64, 33, 34, 54, 39]. These can be construed as *boundaries* between coherent structures, and are therefore of great importance in any transport characterisation. The hyperbolic

| Autonomous, infinite-time | Nonautonomous, infinite-time          | Nonautonomous, finite-time |
|---------------------------|---------------------------------------|----------------------------|
| Saddle fixed points       | Hyperbolic trajectories               | (a)                        |
| Eigenvalues               | Exponential decay rates               | (b)                        |
| Eigenvectors              | Tangents to stable/unstable manifolds | (c)                        |

Table 1: Analogues of important flow entities.

transport templates are characterised in Table 1, and in all these situations, one focus is essentially determining the third column of Table 1, which will be different for each diagnostic method. For the specific case of FTLEs (noting that FTLEs are not always valid [21, 49, 63, 70, 45]), this column would arguably have (a) intersections of forward- and backward-time FTLE ridges<sup>1</sup>, (b) FTLE values, and (c) tangents to FTLE ridges.

Even for nonautonomous infinite-time flows, the definitions in the second column of Table 1 are not easy to apply for detection of these coherent entities. The time-varying hyperbolic trajectories and their stable and unstable manifolds are defined *implicitly*, using the concept of exponential dichotomies [27, 65, 16, 7], which is difficult to use computationally. Methods which would enable easier characterisation and control of these entities would be of value—and in particular, those generalisable to finite-time flows. In this spirit, this article develops techniques which are relevant when the flow is nearly autonomous, that is, when the nonautonomous component appears as a perturbation on an autonomous (steady) flow. A frequently considered assumption in oceanographic and other flows [38, 59, 29], this form of model has additional appeal since it can be considered a particular realisation of a stochastic perturbation, a theme which is attracting considerable recent attention [41, 53, 62]. From the microfluidic perspective, this assumption has value when the idea is to disturb a steady laminar flow (in which transport is suppressed) by imposing an agitation velocity in order to promote transport [72, 76, 75, 10, 9].

Under the nearly-autonomous assumption, it is established in Theorem 2.2 that the analogue of eigenvectors—the directions in which the stable and unstable manifolds emanate at each time instance—can be expressed as a rotation from the autonomous eigenvector directions, with the rotation being governed by a local velocity shear. This result is inverted in Theorem 2.4, where

---

<sup>1</sup>Not all such intersections correspond to hyperbolic trajectories, since homoclinic trajectories are also associated with such intersections.

the control problem of determining the nonautonomous velocity shear needed to make stable and unstable manifolds rotate locally in a prescribed nonautonomous fashion is solved. This result nicely complements already existing results on controlling hyperbolic trajectories [13, 14], and supports the (as yet not easily implementable) first result on controlling stable and unstable manifolds [15]. Since Theorem 2.4 provides the methodology of pointing stable and unstable manifolds in user-desired time-varying directions, this provides insight into how to best focus energy in the most relevant areas, in order to obtain desired mixing characteristics.

A particular desire in establishing the infinite-time nonautonomous results is the ability to generalise them to finite times when entities reminiscent of stable and unstable manifolds appear to be present. (Defining them using exponential dichotomies fails since *anything* can be imputed to be bounded by an exponentially decaying function over finite times; various approaches [28, 49, 30, 17] have been suggested to tackle this.) A common approach for finite times is to consider the flow from a certain fixed initial time to a fixed final time, governed by a specified nonautonomous velocity field [49, 28, 37, 60, 33, 35, 55]. The flow map for this time interval can be obtained computationally, for example, by flowing forward many trajectories, and thereafter transport issues are usually analysed using just this one-step flow map. Nonautonomy is sometimes (but not always) implicit in this approach by allowing either the initial or final time to vary, but this requires performing calculations for differing flow maps [31, 58, 45]. Finite-time reality might be better approximated if assuming that the velocity data is available over a fixed finite-time interval  $[-T, T]$  (possibly at discrete values), but that nonautonomous information is required for times  $t \in (-T, T)$ , using *all* the available data at each instance in time [31]. Under this interpretation, in the nearly autonomous situation, leading-order expressions for the finite-time versions of hyperbolic trajectories and local tangent vectors to their associated stable and unstable manifolds are furnished. This approach effectively supplies an alternative—which generalises stable/unstable manifolds in nearly autonomous flows—to the third column in Table 1. This approach highlights the seldom noticed fact that if data from a finite-time sample  $t \in [-T, T]$  is used to determine invariant manifold-like entities, velocities *outside* the interval could affect the locations of the computed entities. To account for such errors due to lack of data outside the interval  $[-T, T]$ , an error estimate for the tangent vectors, as a function of both  $t$  and  $T$ , is discussed in (25), under the condition of bounded velocity shear.

The theoretical arguments are verified in Section 3, where a nearly autonomous flow is computationally analysed through the generation of spatially and temporally discrete data over a finite time-interval  $[-T, T]$ . This is performed via a two-step analysis: first, the theory is used to determine the nonautonomous velocity for  $t \in (-T, T)$  needed to have hyperbolic trajectories follow user-defined motion, with their stable and unstable manifolds also rotating in a specified time-varying fashion, and second, the data is used to *a posteriori* verify the errors implied by the finite-time definitions. Two different types of nonautonomous perturbations are evaluated: a time-periodic manifold rotation with fairly large nonautonomous part, and an abruptly changing hyperbolic trajectory location and manifold rotation. These examples were chosen to deliberately challenge the expected realm of viability of the theory, but in both cases, excellent results were obtained when compared with FTLE computations. The techniques therefore offer substantial promise in controlling directions of emanation of coherent structure boundaries in finite-time nonautonomous flows, with additional insights into how these directions are related to the local velocity shear.

## 2 Theoretical framework

Consider for  $x \in \Omega \subset \mathbb{R}^2$  the nonautonomous dynamical system

$$\dot{x} = F(x, t, \varepsilon) \tag{1}$$

where the parameter  $\varepsilon \in [0, \varepsilon_0)$  where  $\varepsilon_0 \ll 1$ . The vector field  $F$  is assumed to be defined for  $t \in [-T, T]$  (if  $T < \infty$ ), with (1) being valid for  $t \in (-T, T)$ ; the  $T = \infty$  situation is the classical infinite-time scenario which shall also be addressed. An alternative representation of the nonautonomous flow of (1) is to consider its augmented system

$$\left. \begin{aligned} \dot{x} &= F(x, t, \varepsilon) \\ \dot{t} &= 1 \end{aligned} \right\} \tag{2}$$

in the appended  $\Omega \times (-T, T)$  phase space.

**Hypothesis 2.1.**  $F : \Omega \times (-T, T) \times [0, \varepsilon_0) \rightarrow \mathbb{R}^2$  is such that

(a)  $F \in C_{\text{unif}}^2(\Omega \times (-T, T) \times [0, \varepsilon_0))$ ;

(b) The function  $f(x) := F(x, t, 0)$  is independent of  $t$ ;

(c) *There exists  $a \in \Omega$  such that  $f(a) = 0$ ;*

(d)  *$Df(a)$  has eigenvalues  $\lambda_s$  and  $\lambda_u$  with corresponding normalised eigenvectors  $v_s$  and  $v_u$ , where  $\lambda_s < 0 < \lambda_u$ .*

Some comments on the above hypotheses are in order. Hypotheses 2.1(a) contains basic differentiability and boundedness conditions on  $F$  in relation to  $(x, t, \varepsilon)$ . Recall that the ‘unif’ subscript on the  $C^2$  indicates that all derivatives up to second-order are uniformly bounded. Hypothesis 2.1(b) states that when  $\varepsilon = 0$ ,  $F$  is autonomous, and can be represented by a function  $f(x)$ . Hypotheses 2.1(c,d) guarantee the presence of a hyperbolic fixed point  $a$  associated with this  $f$ , with stable and unstable manifolds emanating in the eigenvector directions  $v_s$  and  $v_u$ , with associated exponential decay rates  $\lambda_s$  and  $\lambda_u$ , respectively. While the normalised  $v_{s,u}$  are only unique up to a negative sign, suppose a particular choice has been made; this effectively chooses one of the two branches of the stable/unstable manifold. When viewed in the appended phase-space of (2), the hyperbolic fixed point  $a$  of (1) transforms to a *hyperbolic trajectory*  $(a, t)$ . An important omission from the hypotheses is that  $F$  be area-preserving; the results will work for compressible as well as incompressible flows.

## 2.1 Analogue of fixed points

What is the analogous entity to  $a$  when  $\varepsilon \neq 0$ ? If using the fixed point characterisation, this might be thought of as a curve of instantaneous fixed/stagnation points  $a(t)$  which satisfies  $F(a(t), t, \varepsilon) = 0$  for any  $t$  and  $\varepsilon$ . While this characterisation continues to be used in some fields, this is well-known to *not* have any significant meaning with regards to fluid transport: these do not follow the Lagrangian flow, are not associated with stable/unstable manifolds, and this characterisation depends on the frame of reference. The governing characteristic of  $a$  of interest is not that it is a fixed point when  $\varepsilon = 0$ , but that *it possesses stable and unstable manifolds*. The analogous entity when  $\varepsilon \neq 0$  is a time-varying trajectory  $a(t)$  which is called a *hyperbolic trajectory*, and whose definition requires *exponential dichotomy conditions* [27, 65, 16] which are extremely difficult to verify in nonautonomous situations. However, Yi’s persistence of integral manifold results [78, 79], building on Hale’s results for more restrictive time-dependence [43], imply the persistence of the  $\varepsilon = 0$  hyperbolic trajectory  $(a, t)$  of (2) as a nearby entity  $(a(t), t)$  when  $\varepsilon \neq 0$ .

The results will be phrased in terms of the ‘nonautonomy’

$$g(x, t, \varepsilon) := F(x, t, \varepsilon) - F(x, t, 0) = F(x, t, \varepsilon) - f(x), \quad (3)$$

which represents how much  $F(x, t, \varepsilon)$  differs from the autonomous vector field  $f(x)$ . By Hypothesis 2.1, there exists a constant  $C$  such that

$$|g(x, t, \varepsilon)| + |Dg(x, t, \varepsilon)| \leq C\varepsilon \quad \text{for } (x, t, \varepsilon) \in \Omega \times (-T, T) \times [0, \varepsilon_0]; \quad (4)$$

i.e.,  $g = \mathcal{O}(\varepsilon)$ . Next, define

$$v_s^\perp := \begin{pmatrix} 0 & -1 \\ 1 & 0 \end{pmatrix} v_s \quad \text{and} \quad v_u^\perp := \begin{pmatrix} 0 & -1 \\ 1 & 0 \end{pmatrix} v_u. \quad (5)$$

which are the vectors  $v_{s,u}$  rotated by  $+\pi/2$ . Thus,  $g$ 's components in the normal directions to the vectors  $v_{s,u}$  can be defined by

$$g_{s,u}^\perp(x, t, \varepsilon) := g(x, t, \varepsilon) \cdot v_{s,u}^\perp. \quad (6)$$

**Theorem 2.1** (‘Fixed point’ movement). *Suppose  $T = \infty$ . The hyperbolic trajectory  $a(t)$  of (1) in relation to  $a$  can be represented by the projections*

$$[a(t) - a] \cdot v_s^\perp = -e^{\lambda_u t} \int_t^\infty e^{-\lambda_u \tau} g_s^\perp(a, \tau, \varepsilon) d\tau + \varepsilon^2 H_s(t, \varepsilon) \quad (7)$$

and

$$[a(t) - a] \cdot v_u^\perp = e^{\lambda_s t} \int_{-\infty}^t e^{-\lambda_s \tau} g_u^\perp(a, \tau, \varepsilon) d\tau + \varepsilon^2 H_u(t, \varepsilon), \quad (8)$$

where there exist  $K_{s,u} > 0$  such that  $|H_{s,u}(t, \varepsilon)| + \left| \frac{\partial H_{s,u}(t, \varepsilon)}{\partial t} \right| \leq K_{s,u}$  for all  $t \in \mathbb{R}$ .

*Proof.* This formulation is a slight modification to Theorem 2.10 by Balasuriya [6], to which the reader is referred to for the proof for the leading-order expression; the bounding of the error term arises from an argument similar to that of Theorem 2.2 which will be shown in detail, and hence will be skipped here.  $\square$

**Remark 2.1.** While Theorem 2.1 gives the *projections* of  $a(t) - a$  to leading-order, an expression for  $a(t)$  could be obtained using elementary trigonometry as [6]

$$a(t) = a + \left[ \alpha_u(t, \varepsilon) v_u^\perp + \frac{\alpha_u(t, \varepsilon) (v_u \cdot v_s) - \alpha_s(t, \varepsilon)}{v_u^\perp \cdot v_s} v_u \right] + \mathcal{O}(\varepsilon^2), \quad (9)$$

where

$$\alpha_s(t, \varepsilon) := -e^{\lambda_u t} \int_t^\infty e^{-\lambda_u \tau} g_s^\perp(a, \tau, \varepsilon) d\tau \quad (10)$$

and

$$\alpha_u(t, \varepsilon) := e^{\lambda_s t} \int_{-\infty}^t e^{-\lambda_s \tau} g_u^\perp(a, \tau, \varepsilon) d\tau. \quad (11)$$

## 2.2 Analogue of eigenvectors

When  $\varepsilon = 0$ , the dynamical system (1) is autonomous, possessing a saddle fixed point  $a$  with eigenvalues  $\lambda_s < 0$  and  $\lambda_u > 0$ , and corresponding normalised eigenvectors  $v_s$  and  $v_u$ . The nonautonomous finite-time version of the fixed point  $a$  has been addressed, and this section approaches the determination of the entities analogous to  $v_{s,u}$ . These are *not* instantaneous eigenvectors (which have no connection to transport templates), but are the directions represented by the local tangent vectors to the stable and unstable manifolds at the point  $a(t)$  at each time  $t$ . It is reasonable to expect the new (time-dependent) tangent vector directions  $v_{s,u}(t)$  to be  $\mathcal{O}(\varepsilon)$ -close to  $v_{s,u}$  in each time-slice  $t$ .

**Theorem 2.2** (‘Eigenvector rotations’). *Suppose  $T = \infty$ . Consider the intersections of the stable and unstable manifolds of  $(a(t), t)$  in a time-slice  $t \in \mathbb{R}$ . The local tangential direction to the stable manifold at the point  $a(t)$  for  $t \in [T_s, \infty)$  for any  $T_s$  can be obtained by an anticlockwise rotation of  $v_s$  by an angle*

$$\theta_s(t) = -e^{(\lambda_u - \lambda_s)t} \int_t^\infty e^{(\lambda_s - \lambda_u)\tau} v_s \cdot \nabla g_s^\perp(a, \tau, \varepsilon) d\tau + \varepsilon^2 E_s(t, \varepsilon), \quad (12)$$

where there exists a constant  $K_s$  such that

$$|E_s(t, \varepsilon)| + \left| \frac{\partial E_s(t, \varepsilon)}{\partial t} \right| \leq K_s \quad \text{for } (t, \varepsilon) \in [T_s, \infty) \times [0, \varepsilon_0].$$

Similarly, the local tangential direction to the unstable manifold at  $a(t)$  at  $t \in (-\infty, T_u]$  for any  $T_u$  is obtained by rotating  $v_u$  by an anticlockwise angle

$$\theta_u(t) = e^{(\lambda_s - \lambda_u)t} \int_{-\infty}^t e^{(\lambda_u - \lambda_s)\tau} v_u \cdot \nabla g_u^\perp(a, \tau, \varepsilon) d\tau + \varepsilon^2 E_u(t, \varepsilon), \quad (13)$$

where there exists a constant  $K_u$  such that

$$|E_u(t, \varepsilon)| + \left| \frac{\partial E_u(t, \varepsilon)}{\partial t} \right| \leq K_u \quad \text{for } (t, \varepsilon) \in (-\infty, T_u] \times [0, \varepsilon_0].$$



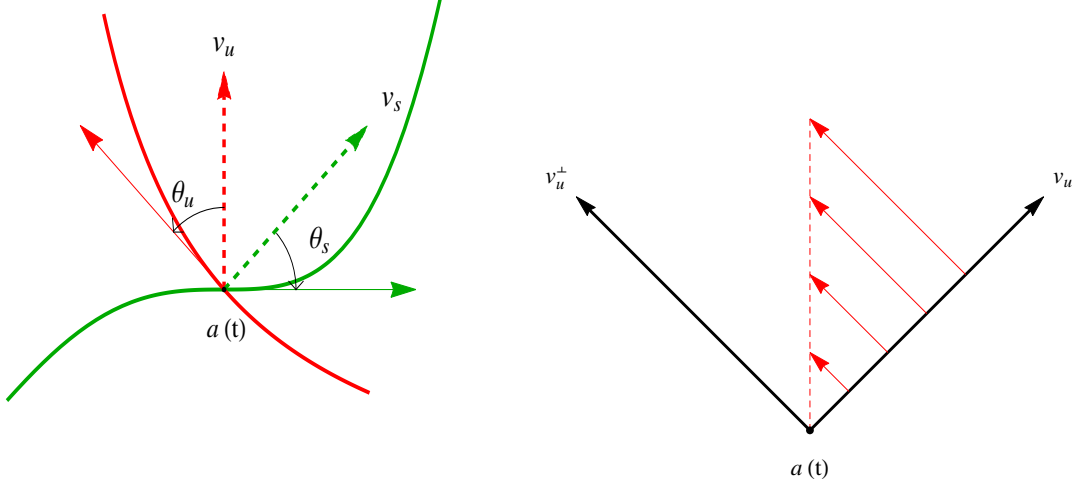


Figure 1: (Left) Tangent vectors to stable (green) and unstable (red) manifolds in a time-slice  $t$ , as expressed by (12) and (13). The dashed arrows are the  $\varepsilon = 0$  eigenvectors. (Right) Illustration of a shear velocity profile tangential to the  $v_u^\perp$  direction which might intuitively be thought to rotate  $v_u$  in the anticlockwise direction.

*Proof.* See Appendix A. □

The angular rotations are illustrated in the left panel of Fig. 1 at a general instance  $t$ . The dashed arrows are the unperturbed eigendirections associated with  $\varepsilon = 0$ , and the tangent vectors to the stable and unstable manifolds are obtained by rotating these anticlockwise by angles  $\theta_{s,u}(t)$ . In the situation pictured in Fig. 1,  $\theta_s(t) < 0$  and  $\theta_u(t) > 0$ .

Additional physical insight into Theorem 2.2 arises from the observation that the key quantity which is being integrated over all relevant time (either backwards or forwards from time  $t$  depending on whether the stable or unstable manifold's tangent vector is being considered) involves a term

$$\sigma_{s,u}(t, \varepsilon) := v_{s,u} \cdot \nabla \left[ g_{s,u}^\perp(a, \tau, \varepsilon) \right]. \quad (14)$$

This is by definition the *shear* of the nonautonomous component of the velocity (i.e., proportional to the shear strain associated with the velocity field  $g$ ) in the  $v_{s,u}^\perp$  directions, since it represents the directional derivative of  $g \cdot v_{s,u}^\perp$  in the direction of  $v_{s,u}$ . For intuition as to why the shear affects the rotation of the tangent vectors, see the right panel of Fig. 1 in which a velocity profile for  $g$  is shown in relation to the  $v_u$  and  $v_u^\perp$  vectors. In this picture,  $g$  is purely in the  $v_u^\perp$  direction, and it is increasing in the coordinate along the  $v_u$  direction. Thus  $\sigma_u$  is positive. However, the velocity

situation in Fig. 1 intuitively will push the further parts of the vector  $v_u$  more than parts near  $a(t)$ , and thus the vector  $v_u$  would be expected to rotate in the anticlockwise direction. This is the positive direction of rotation; positive  $\sigma_u$  corresponds to positive  $\theta_u$ , as is clear from (13). A similar intuition on why the shear rotates  $v_s$  is possible.

**Remark 2.2** (Exponential dichotomy projections). Theorem 2.2 in association with Theorem 2.1 enables an intuitive geometric characterisation of the exponential dichotomy conditions [27, 65, 16] related to the nonautonomous flow (1). First consider  $\varepsilon = 0$ , when  $a$  is a hyperbolic trajectory. Let  $Y(t)$  be a fundamental matrix solution to the linearised flow around  $a$ , i.e.,

$$\dot{y} = Df(a)y, \quad (15)$$

and for convenience choose  $Y(0) = \mathbb{I}$ , the identity. Exponential dichotomies [27, 65, 16] state that in this situation there is a projection  $P$  and constants  $K_{s,u}$  such that

$$\begin{aligned} \|Y(s)PY^{-1}(t)\| &\leq K_s e^{\lambda_s(s-t)} && \text{if } s \geq t, \\ \|Y(s)(\mathbb{I} - P)Y^{-1}(t)\| &\leq K_u e^{\lambda_u(s-t)} && \text{if } s \leq t. \end{aligned} \quad (16)$$

Now, it is easily verified that a solution to (15) which takes the value  $y(t)$  at time  $t$  can be stated as  $y(t) = Y(t)y(0)$  in terms of the fundamental matrix solution. If  $y(0) = Pw$  for any  $w$ , i.e., if  $y(0)$  is in the range of  $P$ , then one can easily use the first exponential dichotomy condition to show that

$$|y(s)| \leq K_s e^{\lambda_s s} |y(0)| \quad \text{for } s \geq 0;$$

see for example Appendix A in [7]. This means that if  $y(0)$  were chosen in  $\mathcal{R}(P)$ , the range of  $P$ , the subsequent solution will decay exponentially with rate  $\lambda_s$ . This solution followed in time will take the form  $y(t) = Y(t)Pw$ , which will therefore lie on the stable fibre, and thus the tangent vector space to the stable manifold at a general time  $t$  is given by  $\mathcal{R}(Y(t)P)$ . This ostensibly depends on time, but for the autonomous equation (15), it actually turns out to not. This is since if  $y(0) = kv_s$  for any  $k$ , then  $y(t) = ke^{\lambda_s t}v_s$ , which continues to be in the same direction as  $v_s$ . Specifically,  $P$  in this case can be defined through  $Pw = (v_s^\top w)v_s$ , and so  $\mathcal{R}(Y(t)P) = \mathcal{R}(v_s)$ . Similarly,  $\mathcal{R}(Y(t)[\mathbb{I} - P]) = \mathcal{R}(v_u)$ , the unstable subspace. Now when  $\varepsilon \neq 0$ , the relevant linearised equation around the hyperbolic trajectory would be

$$\dot{y} = DF(a(t), t)y, \quad (17)$$

which too must satisfy an exponential dichotomy condition such as (16) for its fundamental matrix  $\tilde{Y}(t)$ , but with different (but  $\mathcal{O}(\varepsilon)$ -close) constants  $\tilde{K}_{u,s}$  and  $\tilde{\lambda}_{s,u}$  and projection  $\tilde{P}$ . These are difficult to determine in general. The stable fibres at a general time  $t$  are then given by  $\mathcal{R}\left(\tilde{Y}(t)\tilde{P}\right)$  which now generically depends on  $t$ ; this represents exactly  $\mathcal{R}(v_s(t))$ . The connection to the work in this article is that a unit vector of  $\mathcal{R}\left(\tilde{Y}(t)\tilde{P}\right)$  can be obtained from a unit vector  $v_s$  of  $\mathcal{R}(Y(t)P)$  by rotating by  $\theta_s(t)$ , to leading-order in  $\varepsilon$ . A similar statement holds for the unstable fibres.

**Remark 2.3** (Oseledets spaces). The tangent vectors computed in Theorem 2.2 can also be interpreted as the  $t$ -parametrised basis vectors of the stable and unstable Oseledets spaces [64, 33, 34, 54, 39] associated with the variational equation (17) evaluated at the hyperbolic trajectory. That is, the Oseledets splitting associated with this specific trajectory at time  $t$  is  $\mathcal{R}\left(\tilde{Y}(t)\tilde{P}\right) \oplus \mathcal{R}\left(\tilde{Y}(t)\left[\mathbb{1} - \tilde{P}\right]\right)$ , and this is furnished to leading-order by Theorem 2.2.

### 2.3 Application to finite-time situation

For  $T = \infty$ , it was possible to rigorously define stable and unstable manifolds, and therefore their local tangent vectors were well-defined. If  $T < \infty$ , these cannot be defined in the normal way. Is it possible to modify the results for this situation? Under the nearly autonomous ansatz, this *is* possible in a self-consistent way.

Suppose  $T < \infty$ , and velocity data  $u(x, t)$  is available for  $\Omega \times [-T, T]$ , and there is confidence that the nearly autonomous ansatz is reasonable. For the sake of simplicity we shall still write  $x \in \Omega$  and  $t \in [-T, T]$ , where for typical applications  $x$  will live on some discrete grid over  $\Omega$ , and  $t$  will be a discrete sampling of points in  $[-T, T]$ . It may be possible to decompose  $u(x, t)$  as a sum of a steady and a small unsteady velocity quickly because of prior knowledge (and this is what shall be done in Section 3). If not, a decomposition might be performed as follows, and checked for validity. Define

$$f(x) := \frac{1}{2T} \int_{-T}^T u(x, t) dt \quad \text{and} \quad g(x, t) := u(x, t) - f(x);$$

in these and in other calculations outlined in this section, it is understood that suitable discrete versions (i.e., a Simpson's rule evaluation of the integral above) would be necessary. Letting

$$\|f\| := \sup_{\Omega} |f(x)| \quad \text{and} \quad \|g\| := \sup_{\Omega \times [-T, T]} |g(x, t)|,$$

the data shall be thought of as coming from a nearly autonomous velocity field if the norm of  $g$  is much smaller than the norm of  $f$ . To be specific, the condition for the nearly autonomous ansatz to be valid is that  $\varepsilon := \|g\| \ll \|f\|$ . If so, there is a base steady flow  $f$  which is perturbed though the nonautonomous velocity  $g$ . Under the understanding that  $F(x, t, \varepsilon) = f(x) + g(x, t) = u(x, t)$ , this is consistent with the notation of the previous sections, but  $\varepsilon$  here is a derived parameter, and its presence in  $g$  and  $F$  is hidden. Now,  $g$  is only defined for  $t \in (-T, T)$ , and imagine extending to  $\mathbb{R}$  through

$$\tilde{g}(x, t) = \begin{cases} g(x, t) & \text{if } t \in [-T, T], \\ 0 & \text{if } t \notin [-T, T]. \end{cases} \quad (18)$$

Now consider the *infinite-time* flow

$$\dot{x} = f(x) + \tilde{g}(x, t) \quad (19)$$

for  $(x, t) \in \Omega \times \mathbb{R}$ . What has been done here is that the finite-time nearly autonomous flow has been extended outside the time domain in which data is available, such that the velocity is steady (with a form derived from the dominant characteristics of the available velocity field) outside  $(-T, T)$ . This is a reasonable assumption if the data is obtained from a flow which, for physical or other reasons, is expected to be nearly steady; the ‘averaged’ behaviour outside of which the data is available can then be assumed to be steady, with a form derived from the data itself. Given the infinite-time nature of (19), entities such as hyperbolic trajectories and stable/unstable manifolds are well-defined for the extended flow (19), and Theorems 2.1 and 2.2 apply, subject to the presence of a saddle fixed point  $a$  of  $f$  such that  $Df(a)$  has eigenvalues  $\lambda_s < 0$  and  $\lambda_u > 0$ .

When the nonautonomy is set to zero in this way, there is a strong connection to the scattering theory development by Blazeovski and collaborators [18, 19], who are able to enunciate hyperbolic trajectories and stable/unstable manifolds in terms of diffeomorphisms of the unperturbed entities, where the diffeomorphism is expressed in terms of a ‘scattering map.’ Indeed, they show that for the present perturbative setting, this characterisation is equivalent to a Melnikov approach [18, §3.1], which is the basis for the computations of the present article. These methods which require the nonautonomy to decay to zero as  $t \rightarrow \pm\infty$  at a sufficiently fast rate [18, 19] however do not apply to the infinite-time setting of Sections 2.1–2.2, in which  $F(x, t, \varepsilon)$  need not have such decay.

To compute the leading-order hyperbolic trajectory and stable/unstable manifold tangent vector rotations for (19), one simply needs to set  $g$  to zero outside  $[-T, T]$  in Theorems 2.1 and 2.2.

Theorem 2.1 gives the *leading-order* (in the nonautonomy parameter  $\varepsilon$ ) expression for the hyperbolic trajectory as

$$a^*(t, T) := a + \left[ \alpha_u^*(t, T) v_u^\perp + \frac{\alpha_u^*(t, T) (v_u \cdot v_s) - \alpha_s^*(t, T)}{v_u^\perp \cdot v_s} v_u \right], \quad (20)$$

where

$$\alpha_s^*(t, T) := -e^{\lambda_u t} \int_t^T e^{-\lambda_u \tau} g_s^\perp(a, \tau) d\tau \quad (21)$$

and

$$\alpha_u^*(t, T) := e^{\lambda_s t} \int_{-T}^t e^{-\lambda_s \tau} g_u^\perp(a, \tau) d\tau. \quad (22)$$

Since the original data was for  $t \in [-T, T]$ , and thus the time-derivative would be valid in  $(-T, T)$ , the quantity  $a^*(t, T)$  would give an approximation for the hyperbolic trajectory in the restricted time-domain  $(-T, T)$ . The superscript  $\star$  will be used hereafter to denote leading-order approximations for finite-time analogues of entities.

What if  $g$  is extended in a different way to  $\mathbb{R}$ ? Then the integral limits in (21) and (22) do not get clipped outside  $[-T, T]$ , and thus will lead to a different hyperbolic trajectory to leading-order. If  $g$  is extended to  $\mathbb{R}$  not by setting to zero, but by still following the reasonable hypothesis that  $\|g\| \leq \varepsilon$  (which was true in  $[-T, T]$ ), then the error between using (21) and the correct  $g$ , when projected in the  $v_s^\perp$  direction, is bounded by

$$|A_s^*(t, T)| \leq \varepsilon e^{\lambda_u t} \left| \int_T^\infty e^{-\lambda_u \tau} d\tau \right| = \frac{\varepsilon e^{\lambda_u(t-T)}}{\lambda_u},$$

and similarly  $|A_u^*(t, T)| \leq -\varepsilon e^{\lambda_s(t-T)}/\lambda_s$  for the error in the  $v_u^\perp$  direction. These furnish bounds, to leading-order in the nonautonomous parameter, for possible extensions. This approach of attempting to characterise the effect of velocities from *outside* the interval in which data is available is an important aspect of finite-time analyses which has not been addressed until this, admittedly fairly limited, analysis.

It should be noted that there are several other suggestions for defining finite-time hyperbolic trajectories in terms of exponential dichotomies, since (16) is trivially satisfied when  $t$  is restricted to a finite domain, and so ‘exponentially decaying in finite-time’ would require a stronger condition such as for example insisting on  $K_{s,u} = 1$  [28, 49, 30, 17]. This is a strong restriction. The present approach is an alternative which has applicability if the nonautonomy is small, and if there is sufficient confidence in the fact that the velocity does not change unduly outside the interval in which data is available.

By using the extension (18) and the infinite-time flow (19), stable and unstable manifolds are well-defined, and therefore so are their location tangent vectors. Using Theorem 2.2, their directions in a time-slice  $t \in (-T, T)$ , to leading-order in the nonautonomous parameter, will be given by anticlockwise rotational angles

$$\theta_s^*(t, T) := -e^{(\lambda_u - \lambda_s)t} \int_t^T e^{(\lambda_s - \lambda_u)\tau} v_s \cdot \nabla g_s^\perp(a, \tau) d\tau \quad (23)$$

and

$$\theta_u^*(t, T) := e^{(\lambda_s - \lambda_u)t} \int_{-T}^t e^{(\lambda_u - \lambda_s)\tau} v_u \cdot \nabla g_u^\perp(a, \tau) d\tau. \quad (24)$$

of  $v_s$  and  $v_u$  respectively. As  $\theta_s^*(T, T) = \theta_u^*(-T, T) = 0$ , the stable and unstable finite-time tangent vectors evolve smoothly in  $(-T, \infty)$  and  $(-\infty, T)$  respectively. One inevitable factor in this process is that since the data was only available on  $[-T, T]$ , the ‘guess’ used for the data outside  $[-T, T]$  will affect the computed stable and unstable manifolds. As shown by Sandstede et al [69], the errors resulting from extending  $g$  outside  $(-T, T)$  in a nontrivial but bounded way would imply that the invariant manifolds can only be characterised as ‘fat curves;’ such nonuniqueness for finite time has also been identified and discussed in alternative ways [47, 59, 7, 22].

In what way can the fact that the data is limited to a finite time domain be used to characterise how the flow entities would change *if data were available from outside the interval?* After all, in many problems, practitioners are forced to work with a finite-time data set over some interval, when of course the Lagrangian flow has been/will be impacted by velocities from outside that interval which are not available. This is indeed examined in Section 3 and compared with numerical computations, in a situation when  $\theta_s(t)$  is known. In general, it may not be. Consider, then, a situation in which  $g$  is extended outside of  $(-T, T)$  in a nontrivial, but still ‘reasonable’ way, of letting the velocity shear be bounded in the form  $|\sigma_{s,u}(t)| \leq \varepsilon S$  for all  $t \in \mathbb{R}$ . The errors in using the zero- $g$  approximations can then be approximated. If  $E_{s,u}^*(t, T) := \theta_{s,u}^*(t, T) - \theta_{s,u}(t, \infty)$ , then

$$E_s^*(t, T) = e^{(\lambda_u - \lambda_s)t} \int_T^\infty e^{(\lambda_s - \lambda_u)\tau} \sigma_s(\tau) d\tau$$

and

$$E_u^*(t, T) = -e^{(\lambda_s - \lambda_u)t} \int_{-\infty}^{-T} e^{(\lambda_u - \lambda_s)\tau} \sigma_u(\tau) d\tau.$$

from which it is possible to determine the error bounds

$$|E_s^*(t, T)| \leq \frac{\varepsilon S e^{(\lambda_u - \lambda_s)(t-T)}}{\lambda_u - \lambda_s} \quad \text{and} \quad |E_u^*(t, T)| \leq \frac{\varepsilon S e^{(\lambda_s - \lambda_u)(t+T)}}{\lambda_u - \lambda_s}. \quad (25)$$

Generically, exponential decay is to be expected in the finiteness parameter  $T$ , with rate given by the *difference in the eigenvalues*. Since to leading-order these are approximated by forward and backwards time finite-time Lyapunov exponents which can be computed from the data, (25) gives a method for estimating the behaviour of the error due to the finiteness  $T$  of the data.

## 2.4 Nonautonomously controlling manifold directions

This section addresses the inverse question of determining the velocity required to ensure that the stable and unstable manifolds rotate nonautonomously by specified time-varying angles. Consider determining the control velocity  $c(x, t)$  such that

$$\dot{x} = f(x) + c(x, t) \quad (26)$$

moves the hyperbolic trajectory from  $a$  to a *specified* nearby time-varying location  $\tilde{a}(t)$ , and simultaneously rotates the eigenvectors  $v_{s,u}$  associated with  $c(x, t) \equiv 0$  by *specified*, nonautonomously changing, small angles  $\tilde{\theta}_{s,u}(t)$ .

**Theorem 2.3** (Controlling hyperbolic trajectory location [13]). *Let  $T = \infty$ , and suppose (26) with  $c(x, t) \equiv 0$  has a saddle fixed point  $a$  with eigensystem  $\{\lambda_{s,u}, v_{s,u}\}$ . Let  $\tilde{a}(t)$  be specified such that  $|\tilde{a}(t) - a| + |\tilde{a}'(t)| \leq \varepsilon$  for all  $t \in \mathbb{R}$ . If  $c(x, t)$  is chosen such that*

$$\left. \begin{aligned} c(a, t) \cdot v_s^\perp &= [\tilde{a}'(t) - \lambda_u(\tilde{a}(t) - a)] \cdot v_s^\perp \\ c(a, t) \cdot v_u^\perp &= [\tilde{a}'(t) - \lambda_s(\tilde{a}(t) - a)] \cdot v_u^\perp \end{aligned} \right\}, \quad (27)$$

and also subject to the presence of  $A$  such that

$$|c(x, t)| + |Dc(x, t)| + \left| \frac{\partial c(x, t)}{\partial t} \right| \leq \varepsilon A \quad \text{for } (x, t) \in \Omega \times \mathbb{R},$$

then there is a  $K$  and an actual hyperbolic trajectory  $a(t)$  of (26) such that

$$|\tilde{a}(t) - a(t)| \leq \varepsilon^2 K \quad \text{for all } t \in \mathbb{R}.$$

*Proof.* This result already appears in the literature in a slightly different form [13]; formal methods for achieving higher-order accuracy [14], or of stabilising the trajectory [77] are also available.  $\square$

Theorem 2.3 relates to ‘inverting’ Theorem 2.1. Of note here is the fact that there is no  $\varepsilon$  explicit to the velocity field, but rather  $\varepsilon$  is a parameter representing how large the deviation of

the required hyperbolic trajectory  $\tilde{a}$  is from the uncontrolled hyperbolic fixed point  $a$ . Under the specified form (27) of the control velocity, the difference between the desired and actual hyperbolic trajectories will then be of order  $\varepsilon^2$ . Of course, this result will only be useful if  $\varepsilon$  is sufficiently small. Next, the main contribution of this article towards a control strategy—manipulating the directions at which the stable and unstable manifold emanate—is stated.

**Theorem 2.4** (Controlling manifold directions). *Under the hypotheses of Theorem 2.3, suppose also  $\tilde{\theta}_{s,u} : \mathbb{R} \rightarrow \mathbb{R}$  such that  $|\tilde{\theta}_{s,u}(t)| + |\tilde{\theta}'_{s,u}(t)| < \varepsilon$  for all  $t$ . If  $c(x, t)$  is chosen subject to the velocity shear conditions*

$$v_s \cdot \nabla \left[ c(x, t) \cdot v_s^\perp \right] \Big|_{x=a} = \tilde{\theta}'_s(t) - (\lambda_u - \lambda_s) \tilde{\theta}_s(t) \quad (28)$$

and

$$v_u \cdot \nabla \left[ c(x, t) \cdot v_u^\perp \right] \Big|_{x=a} = \tilde{\theta}'_u(t) + (\lambda_u - \lambda_s) \tilde{\theta}_u(t), \quad (29)$$

and also subject to the presence of  $A$  such that

$$|c(x, t)| + |Dc(x, t)| + \left| \frac{\partial c(x, t)}{\partial t} \right| \leq \varepsilon A \quad \text{for } (x, t) \in \Omega \times \mathbb{R}, \quad (30)$$

then there exist  $K_{s,u}$  such that the actual rotational angles  $\theta_{s,u}(t)$  of the stable and unstable manifolds at the hyperbolic trajectory location  $a(t)$  of (26) satisfy

$$\begin{aligned} |\theta_s(t) - \tilde{\theta}_s(t)| &\leq \varepsilon^2 K_s \quad \text{for } t \in [T_s, \infty) \quad \text{and} \\ |\theta_u(t) - \tilde{\theta}_u(t)| &\leq \varepsilon^2 K_u \quad \text{for } t \in (-\infty, T_u], \end{aligned}$$

for any finite  $T_{s,u}$ .

*Proof.* Note that (26) is the same as (1) under the identification  $F(x, t, \varepsilon) = f(x) + c(x, t)$ , and thus  $g(x, t, \varepsilon) = c(x, t)$ . However, there is no explicit  $\varepsilon$ -dependence in the vector field, which is only proper given that no such  $\varepsilon$ -dependence was specified in the required rotations, save for the fact that these rotations are of *maximum* size  $\varepsilon$ . The condition on the size of  $c$  and its spatial and temporal derivative (30) is stronger than the requirement for  $g$ , and thus the result of Theorem 2.2 applied to this  $c$  leads to

$$\theta_s(t) = -e^{(\lambda_u - \lambda_s)t} \int_t^\infty e^{(\lambda_s - \lambda_u)\tau} \sigma_s(\tau) d\tau + \varepsilon^2 E_s(t, \varepsilon)$$

for  $t \in [T_s, \infty)$  for the *actual* rotation of the local stable manifold, where from (14),

$$\sigma_s(t) = v_s \cdot \nabla \left[ c(x, t) \cdot v_s^\perp \right] \Big|_{x=a}.$$



Therefore,

$$e^{(\lambda_s - \lambda_u)t} \theta_s(t) = - \int_t^\infty e^{(\lambda_s - \lambda_u)\tau} \sigma_s(\tau) d\tau + \varepsilon^2 E_s(t, \varepsilon) e^{(\lambda_s - \lambda_u)t},$$

which upon differentiating with respect to  $t$  gives

$$e^{(\lambda_s - \lambda_u)t} [\theta'_s(t) + (\lambda_s - \lambda_u) \theta_s(t)] = e^{(\lambda_s - \lambda_u)t} \sigma_s(t) + \varepsilon^2 e^{(\lambda_s - \lambda_u)t} \left[ \frac{\partial E_s(t, \varepsilon)}{\partial t} + (\lambda_s - \lambda_u) E_s(t, \varepsilon) \right].$$

The actual velocity shear is therefore

$$\sigma_s(t) = \theta'_s(t) + (\lambda_s - \lambda_u) \theta_s(t) - \varepsilon^2 \left[ \frac{\partial E_s(t, \varepsilon)}{\partial t} + (\lambda_s - \lambda_u) E_s(t, \varepsilon) \right],$$

in terms of the *actual* rotation angle  $\theta_s$ . On the other hand, the control velocity was chosen subject to (28) and hence

$$\tilde{\theta}'_s(t) + (\lambda_s - \lambda_u) \tilde{\theta}_s(t) = \theta'_s(t) + (\lambda_s - \lambda_u) \theta_s(t) - \varepsilon^2 \left[ \frac{\partial E_s(t, \varepsilon)}{\partial t} + (\lambda_s - \lambda_u) E_s(t, \varepsilon) \right].$$

Upon defining  $\eta(t) := \tilde{\theta}_s(t) - \theta_s(t)$ , the differential equation

$$\eta'(t) + (\lambda_s - \lambda_u) \eta(t) = -\varepsilon^2 \left[ \frac{\partial E_s(t, \varepsilon)}{\partial t} + (\lambda_s - \lambda_u) E_s(t, \varepsilon) \right] =: \varepsilon^2 \tilde{E}_s(t, \varepsilon)$$

results, where by Theorem 2.2,  $\tilde{E}_s(t, \varepsilon)$  is bounded on  $[T_s, \infty)$ . Multiplying by the integrating factor and integrating from a general time  $t > T_s$  to  $\infty$  yields

$$\lim_{\tau \rightarrow \infty} \left[ e^{(\lambda_s - \lambda_u)\tau} \eta(\tau) \right] - e^{(\lambda_s - \lambda_u)t} \eta(t) = \varepsilon^2 \int_t^\infty e^{(\lambda_s - \lambda_u)\tau} \tilde{E}_s(\tau, \varepsilon) d\tau.$$

The limit on the left is zero because  $\theta$  and  $\tilde{\theta}$ , and consequently  $\eta$ , are bounded on  $[T_s, \infty)$ , and  $\lambda_s - \lambda_u < 0$ . By virtue of the bound (call it  $\tilde{K}_s$ ) of  $\tilde{E}$ ,

$$e^{(\lambda_s - \lambda_u)t} |\eta(t)| \leq \varepsilon^2 \tilde{K}_s \int_t^\infty e^{(\lambda_s - \lambda_u)\tau} d\tau = \varepsilon^2 \frac{\tilde{K}_s e^{(\lambda_s - \lambda_u)t}}{\lambda_u - \lambda_s},$$

and therefore  $|\eta(t)| \leq \varepsilon^2 \tilde{K}_s / (\lambda_u - \lambda_s) =: \varepsilon^2 K_s$ , proving that the actual and the desired rotations are bounded by an  $\mathcal{O}(\varepsilon^2)$  quantity for  $t \in [T_s, \infty)$ . The development so far was only for the rotation of the stable manifold; the expression (29) is similarly derived from (13).  $\square$

Theorem 2.4 shows that the analogue of eigenvectors can be controlled via imposing a prescribed velocity shear. The proof strategy above is similar to that previously used to control the hyperbolic trajectory locations [13]; this has now been extended to be able to also control the directions of emanation of invariant manifolds.

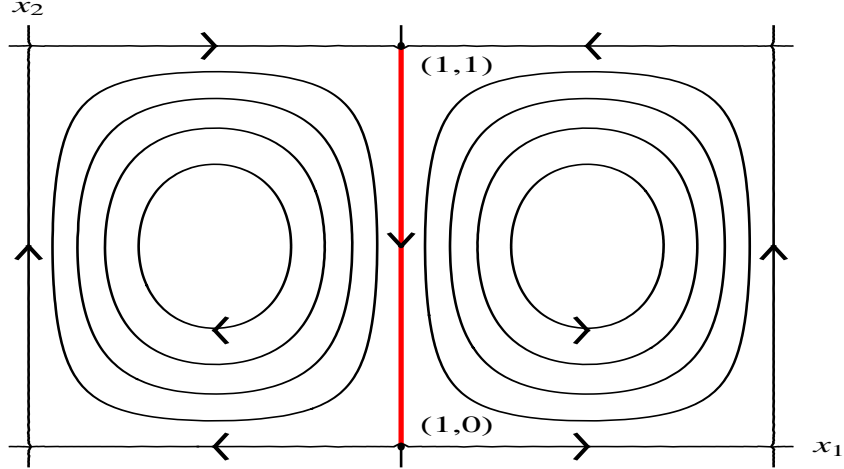


Figure 2: The Taylor-Green flow (31); the key entity [heavy line] is the heteroclinic connection from  $(1, 1)$  to  $(1, 0)$ .

**Remark 2.4** (Finite-time control of manifold directions). Let  $T < \infty$ , and suppose  $\tilde{\theta}_{s,u}^*(t)$  is only specified for  $t \in (-T, T)$ . Then, by choosing  $\tilde{\sigma}_{s,u}^*(t)$  for  $t \in (-T, T)$  as in Theorem 2.4, the expectation is that corresponding finite-time stable and unstable manifolds will emanate in the directions specified by  $\theta_{s,u}^*(t)$  to leading-order in the nonautonomy parameter. However, the finiteness *will* contribute to a  $\mathcal{O}(\varepsilon)$  error; see (25), for example.

### 3 Implementation and verification

This section numerically investigates the theory of the previous sections, specifically focussing on a finite-time setting. Firstly, a control condition on how the manifolds emanate is considered, and then numerically evaluated using finite-time Lyapunov exponents. Secondly, the influence of finiteness of time is assessed. The system chosen for investigation is the well-known Taylor-Green flow [25, 73, 4]

$$\left. \begin{aligned} \dot{x}_1 &= -\pi A \sin(\pi x_1) \cos(\pi x_2) \\ \dot{x}_2 &= \pi A \cos(\pi x_1) \sin(\pi x_2) \end{aligned} \right\} \quad (31)$$

whose phase portrait (Fig. 2) has a stable manifold coming vertically downwards to the saddle fixed point  $(1, 0)$ , which is simultaneously a branch of the unstable manifold emanating downwards

from the point  $(1, 1)$ . The relevant eigenvalues are  $\pm\pi^2 A$  at both these points. The break up of these stable and unstable manifolds under a perturbation results in transport between the left gyre  $[0, 1] \times [0, 1]$  and the right gyre  $[1, 2] \times [0, 1]$ .

Being able to simultaneously control the two splitting manifolds has an impact on the transport between the two gyres. Suppose a finite-time nonautonomous perturbation is to be introduced to (31) such that the local stable and unstable manifolds rotate by angles  $\tilde{\theta}_s(t)$  and  $\tilde{\theta}_u(t)$  respectively, and the hyperbolic trajectories perturbing from  $(1, 0)$  and  $(1, 1)$  also follow a specified time-variation, where the variations of these from the unperturbed situation is bounded by  $\varepsilon$ . If  $c = (c_1 \ c_2)^\top$  is the control perturbation which achieves this subject to an error which is bounded according to Theorems 2.3 and 2.4, the system is now

$$\left. \begin{aligned} \dot{x}_1 &= -\pi A \sin(\pi x_1) \cos(\pi x_2) + c_1(x_1, x_2, t) \\ \dot{x}_2 &= \pi A \cos(\pi x_1) \sin(\pi x_2) + c_2(x_1, x_2, t) \end{aligned} \right\}. \quad (32)$$

Applying Theorem 2.4 for the stable manifold of the hyperbolic trajectory near  $(1, 0)$  leads to

$$\frac{\partial c_1}{\partial x_2}(1, 0, t) \approx - \left[ \tilde{\theta}'_s(t) - 2\pi^2 A \tilde{\theta}_s(t) \right],$$

and a similar analysis for the unstable manifold of the hyperbolic trajectory near  $(1, 1)$  yields

$$\frac{\partial c_1}{\partial x_2}(1, 1, t) \approx - \left[ \tilde{\theta}'_u(t) + 2\pi^2 A \tilde{\theta}_u(t) \right].$$

### 3.1 Time-periodic example

First, suppose that the hyperbolic trajectories are required to remain at their autonomous locations, but that the stable and unstable manifold are to be moved in a time-periodic fashion. From Theorem 2.3, it is clear that choosing  $c_{1,2}(1, 0, t) = 0$  and  $c_{1,2}(1, 1, t) = 0$  makes the leading-order hyperbolic trajectory movement zero. While complying with this, the required rotations of the tangent vectors can be realised by choosing  $c_2(x_1, x_2, t) \equiv 0$  and

$$c_1(x_1, x_2, t) = - \left[ \tilde{\theta}'_s(t) - 2\pi^2 A \tilde{\theta}_s(t) \right] x_2 I_{(1,0)}(x_1, x_2) - \left[ \tilde{\theta}'_u(t) + 2\pi^2 A \tilde{\theta}_u(t) \right] (x_2 - 1) I_{(1,1)}(x_1, x_2) \quad (33)$$

where

$$I_{(x_1^0, x_2^0)}(x_1, x_2) = \frac{1}{2} \left[ \tanh \frac{\sqrt{(x_1 - x_1^0)^2 + (x_2 - x_2^0)^2} + \delta}{\delta^2} - \tanh \frac{\sqrt{(x_1 - x_1^0)^2 + (x_2 - x_2^0)^2} - \delta}{\delta^2} \right]$$

is used as a smoothed version of an indicator function in an  $\delta$ -radius ball around  $(x_1^0, x_2^0)$ . Now, if  $\theta_s$  and  $\theta_u$  are both positive, the stable and unstable manifolds will respectively emanate towards the left gyre and the right gyre. Any subsequent intersection pattern between them will then span a larger area than if the manifolds emanated into the *same* gyre. Since this intuition translates to whenever  $\theta_s$  and  $\theta_u$  have the same sign, one method for attempting to achieve greater transport would be to have  $\tilde{\theta}_{s,u}(t)$  oscillating in phase. To achieve this, choose  $\tilde{\theta}_{s,u}(t) = \delta \cos(\omega t)$ , and thus one can take the bound in Theorem 2.4 to be  $\varepsilon = \delta(1 + |\omega|)$ . This gives the control velocity

$$\begin{pmatrix} c_1(x_1, x_2, t) \\ c_2(x_1, x_2, t) \end{pmatrix} = \delta \begin{pmatrix} [\omega \sin(\omega t) + 2\pi^2 A \cos(\omega t)] x_2 I_{(1,0)}(x_1, x_2) \\ + [\omega \sin(\omega t) - 2\pi^2 A \cos(\omega t)] (x_2 - 1) I_{(1,1)}(x_1, x_2) \\ 0 \end{pmatrix}. \quad (34)$$

To evaluate this method *in finite time*, the choice of parameters  $A = 1$  and  $\omega = 2\pi$  is used, and thus  $\varepsilon = \delta(1 + 4\pi)$ . The finiteness parameter is chosen as  $T = 2$ , which is double the period of  $c_1$ , and therefore not very large. The value  $\delta = 0.2$  is chosen to deliberately examine the efficacy of the method at relatively large  $\varepsilon$  (which is  $0.2(1 + 4\pi) \approx 2.71$  in this case, in comparison to the unperturbed velocity scale of  $\pi A \approx 3.14$ ) at which the perturbative nature of the theory may be compromised. A temporal discretisation using 101 time-slices was used for the time-interval  $[-2, 2]$  with a time-spacing of 0.04. FTLE fields were then calculated within each time-slice numerically<sup>2</sup>, but using the *full* data available at each instance. For example, when considering the time-slice  $t = 0.44$ , forward FTLEs included data from  $t = 0.44$  to  $t = 2.0$  (a time-interval of length 1.56) while backward FTLE used data from  $t = -2.0$  to 0.44 (a time-length of 2.44). This is in keeping with the understanding that, given a certain finite-time data set, one would like to use the maximum information available in that set in performing numerical calculations. FTLEs were chosen as the diagnostic for finite-time versions of stable and unstable manifolds since when focussing near the relevant point, their ridges appeared unambiguously. Thus, technical modifications to counteract possible misdiagnoses by FTLEs [21, 51, 71, 63, 70, 44] were not needed. Moreover, FTLEs in their simplest sense are possibly the most commonly used diagnostic method in the literature, even though other methods, or suitable refinements of existing methods [45, 50, 61, 1, 24, 32, e.g.], continue to be developed. The results for  $t = 0$  are shown in Fig. 3, which shows the angular

---

<sup>2</sup>FTLE computations were performed using LCS Matlab kit Version 2.3 developed at the Biological Propulsion Laboratory, CalTech, and available at: <http://dabiri.caltech.edu/software.html>.

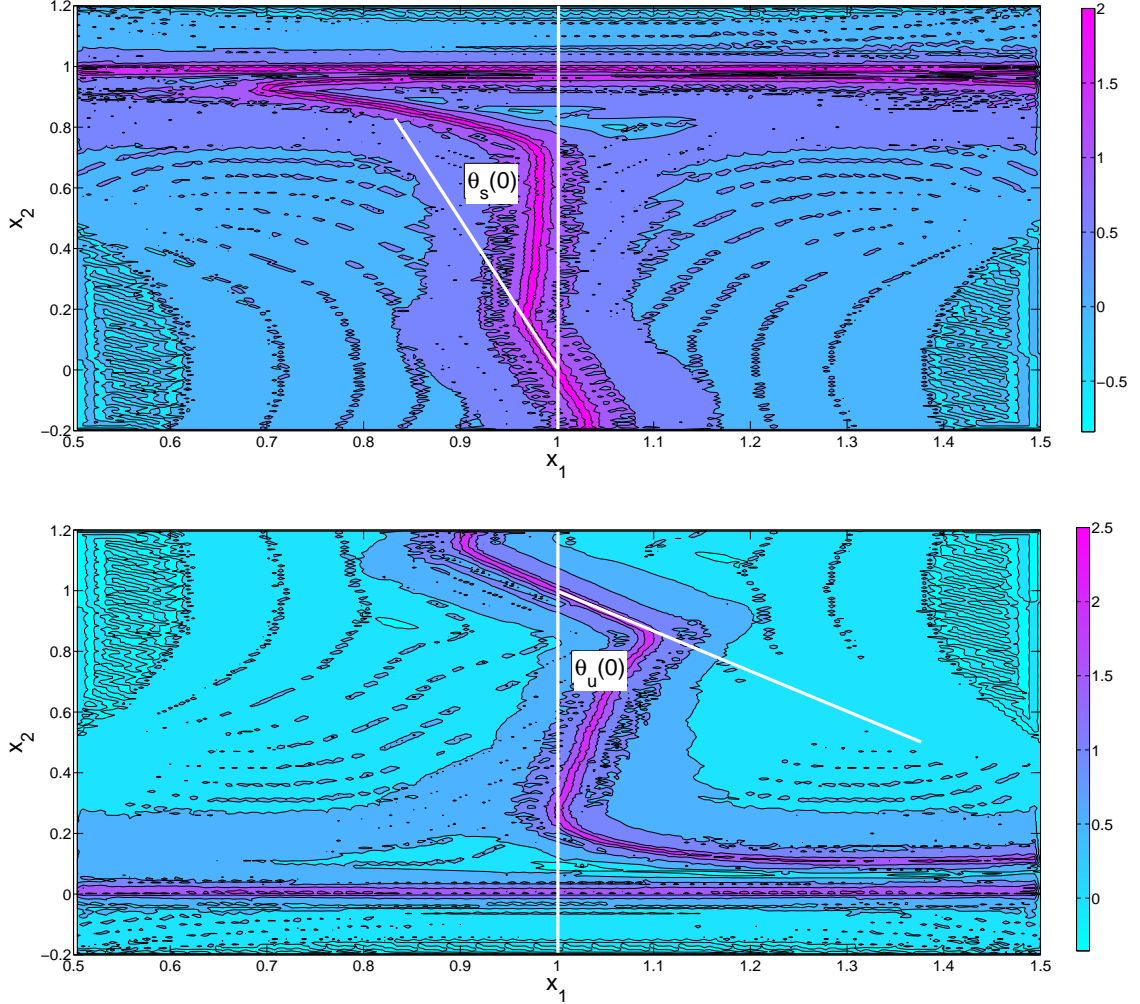


Figure 3: Forward-time (top) and backward-time (bottom) FTLEs at  $t = 0$  for the finite-time control velocity (34), with  $A = 1$ ,  $\omega = 2\pi$ ,  $\delta = 0.2$  and  $T = 2$ .

rotations  $\theta_{s,u}(0)$  incurred by the clearly defined FTLE ridges. Thus by focussing energy in  $\delta$ -balls around  $(1, 0)$  and  $(1, 1)$  in a judiciously selected fashion, global transport has therefore been enhanced.

Henceforth, attention will be focussed on evaluating the accuracy of the stable manifold. At each  $t$  value, points on the Lyapunov exponent ridge were extracted by zeroing in to the region  $-0.04 < x_2 < 0.04$  in the vicinity of  $(1, 0)$ , and picking points from the FTLE field which lie above a cut-off threshold (0.95 of the maximum FTLE value). This simple-minded ridge-extraction algorithm is sufficient for the purposes of computations in this article, since a dominant ridge is

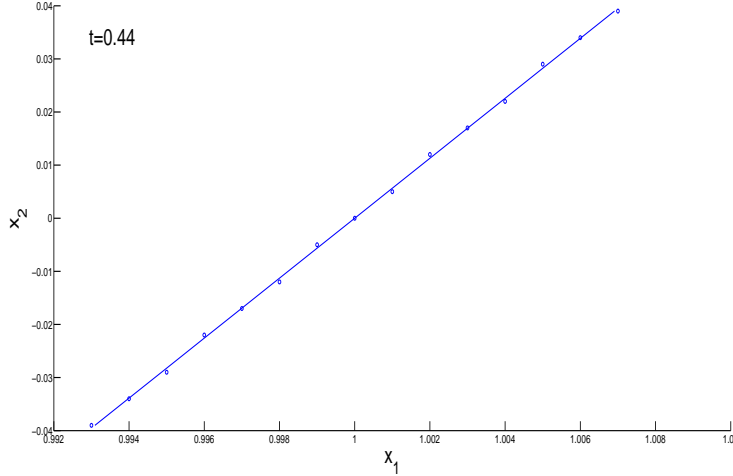


Figure 4: Points on the extracted FTLE ridge [circles] near  $(1, 0)$  in the time-slice  $t = 0.44$ ; the corresponding linear fit is shown by the straight line.

present in the vicinity of  $(1, 0)$ ; if not, more sophisticated approaches would be necessary [51, 70]. An example is shown for  $t = 0.44$  in Fig. 4; the points essentially lie along a straight line which, in this case, corresponds to a negative  $\theta_s$  since the rotation is clockwise from the vertical. The slope and intercept of this line were calculated using standard linear regression. The negative reciprocal of the slope gives  $\tan \theta_s$ , while the intercept can be used to compute the location of the perturbed hyperbolic trajectory. The  $x_1$  coordinate of the hyperbolic trajectory variation with  $t$  is shown in the left panel of Fig. 5. This is preserved near  $x_1 = 1$  with very high accuracy, as expected with the choice of  $c_1 = c_2 = 0$  at  $(1, 0)$  and Theorem 2.1. The values of the computed  $\theta_s$ s from the FTLE ridge extraction procedure are displayed in the right panel of Fig. 5 as circles, for  $t$  values in  $[0, 1]$ . The numerical calculations were performed independently at each  $t$  value, to not prejudice their comparison to the desired tangent vectors at independent times, rather than using improvements to FTLE ideas [50] in which Lagrangian advection of FTLE ridges can be used to advantage. These computed values of  $\theta_s(t)$  are remarkably close to the specified curve  $\tilde{\theta}_s(t) = \delta \cos(\omega t)$ , illustrating that the control strategy used is highly effective even at this relatively large value of  $\varepsilon$ . This offers evidence that (23) and (24) offer excellent approximations in this case.

The theoretical results indicated that the error would be of order  $\varepsilon^2$ , which since  $\varepsilon = \delta(1 + 4\pi)$  is equivalent to the statement that it is of order  $\delta^2$  in this situation. To test this, the quantity  $E =$

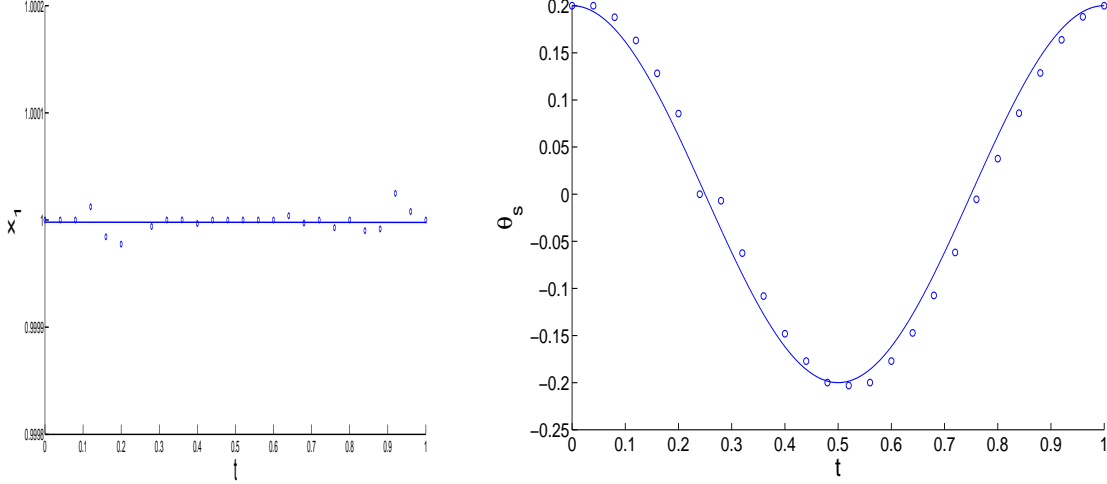


Figure 5: Results for the control velocity (34) with  $\delta = 0.2$ ,  $A = 1$ ,  $\omega = 2\pi$  and  $T = 2$ , extracted by computing the intercept and slope of the FTLE ridges using linear regression [circles]:  $x_1$ -coordinate of hyperbolic trajectory (left panel) and  $\theta_s$  (right panel) in comparison with the expected curves [solid].

$\left| \tilde{\theta}_s(0) - \theta_s(0) \right|$  where  $\theta_s(0)$  is that computed via the FTLE ridges and their slopes, was determined for different values of  $\delta$ . The results are shown in the log-log plot of Fig. 6. While the log-log plot only approximately a straight line, it indicates that the error is approximately  $\mathcal{O}(\varepsilon^{2.5})$ , which is consistent with Theorem 2.2. It was observed that the spatial grid resolution is unable to see the perturbation if  $\delta \lesssim 0.2$ , below which the numerical computations return  $\theta_s(0) = 0$ . A more refined grid will be necessary to push the calculations to smaller  $\delta$ s, resulting in significant computational cost.

Next, the evaluation of the error as a consequence of clipping the data at a finite  $T$  was performed. In keeping with finite-time reality, all the FTLE computations were run up to time  $T = 2$ , the largest value of time for which data was considered available. Thus each data point in Fig. 5 was computed by flowing forward over a *different* amount of time ( $T - t$  for differing values of  $t$ ). Assuming that the vector field is only defined up to time  $T$ , simplifying (23) with these parameters and the desired  $\tilde{\theta}_s$  gives the leading-order *finite-time* rotation of the stable manifold to be

$$\tilde{\theta}_s^*(t, T) = \delta \cos(\omega t) - \delta e^{-2\pi^2 A(T-t)} \cos(\omega T) ,$$

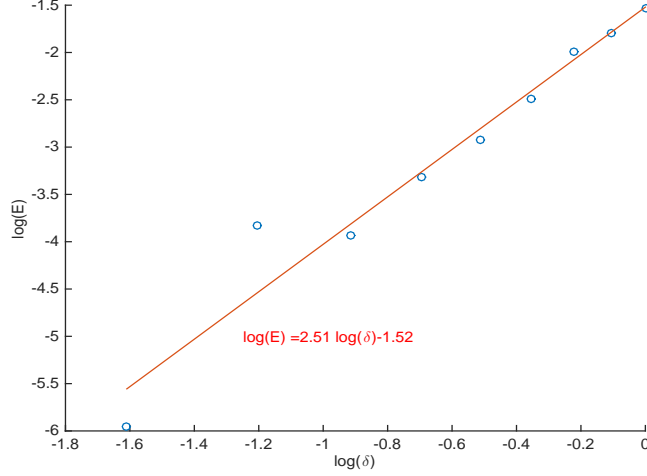


Figure 6: Asymptotic order error analysis for the control velocity (34) with  $A = 1$ ,  $\omega = 2\pi$  and  $T = 1$ , where  $E = \left| \tilde{\theta}_s(0) - \theta_s(0) \right|$ , displaying that  $E \sim \mathcal{O}(\delta^{2.5}) = \mathcal{O}(\varepsilon^{2.5})$ .

whereas the infinite-time leading-order value is  $\theta(t) = \delta \cos \omega t$ . Therefore, the error related to the finiteness of  $T$  is

$$E_s^*(t, T) := \tilde{\theta}_s^*(t, T) - \theta_s(t) = -\delta e^{-2\pi^2 A(T-t)} \cos(\omega T), \quad (35)$$

which gives a estimate—based on the *desired* rotation  $\tilde{\theta}_s$ —of how the stable manifold rotation to leading-order in the nonautonomy is impacted by clipping the data at different  $T$  values. If fully infinite-time data ( $T = \infty$ ) is available, the leading-order error goes to zero. If data from a clipped time  $[-T, T]$  is used, the leading-order in  $\varepsilon$  (equivalently, in  $\delta$ ) stable manifold rotation incurs an error characterised by (35). Let  $t = 0$  be fixed. For  $T$  values in the range 0.2 to 1.0 in steps of 0.04, the forward time FTLE can be computed using data in the interval  $[0, T]$ . For each such  $T$ , the actual  $\theta_s^*(0, T)$  was computed numerically using the ridge extraction procedure and linear regression, as described before. The important thing to note is that during each computation, the data is only assumed to be known in the interval  $[0, T]$ , which is different for each  $T$ . Since  $\theta_s(0) = \delta \cos(\omega 0) = \delta$ , the estimate for  $\theta_s^*(0, T) - \theta_s(0)$  can be found from the data, which is pictured by the filled circles in Fig. 7. The curve in Fig. 7 is the right-hand side of (35) with  $t = 0$ ; the differences between the curve and the circles is because the curve uses the *desired* value  $\tilde{\theta}_s$  whereas the circles are the *obtained* values of  $\theta_s$ .



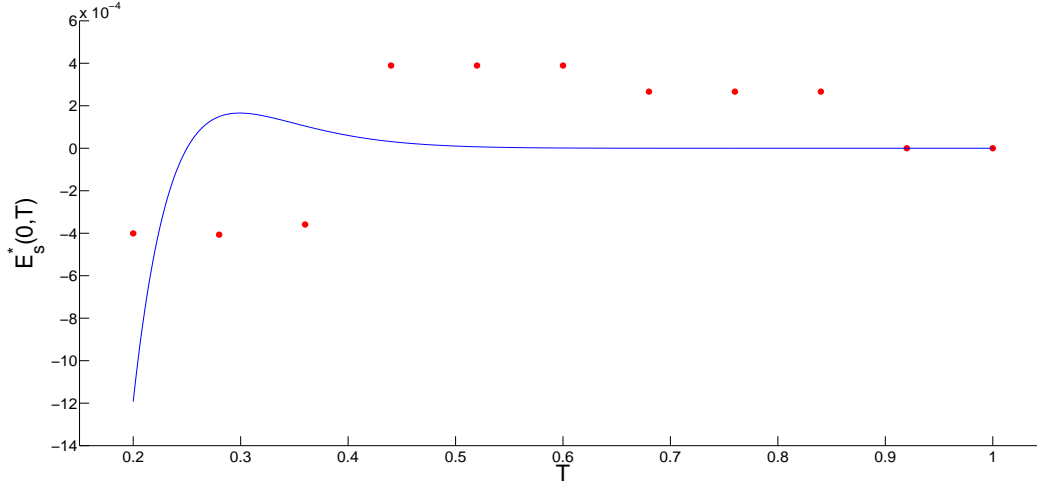


Figure 7: Numerically computed values of  $\theta_s^*(0, T) - \theta_s(0)$  [filled circles], compared with the error estimate (35) [solid curve], with  $\delta = 0.2$ ,  $A = 1$  and  $\omega = 2\pi$ .

### 3.2 Time-discontinuous example

Time-periodicity is not a requirement of the theory. In order to push this advantage further than one could legitimately hope, suppose

$$\tilde{a}(t) = (1 + \delta(4t-2) [H(t-1/4) - H(t-3/4)], 0)^\top \quad \text{and} \quad \tilde{\theta}_s(t) = \delta [1 - H(t-1/2)] \quad (36)$$

where  $H(\cdot)$  is the Heaviside function, and  $\delta > 0$  a parameter. This ambitious requirement does *not* comply with theoretical conditions needed; the bound  $\varepsilon$  arising from  $\tilde{a}$ ,  $\tilde{\theta}_s$  and their derivatives in Theorems 2.3 and 2.4 does not exist at some points. Moreover, abrupt switching of locations cannot be achieved in smooth differential equations, and indeed the definition of a stable manifold collapses. How well can the theory be used to help to achieve these computationally?

Choose smoothed versions of (36) given by

$$\tilde{a}(t) = \left( 1 + \delta(2t-1) \left[ \tanh\left(\frac{t-1/4}{\delta^2}\right) - \tanh\left(\frac{t-3/4}{\delta^2}\right) \right], 0 \right)^\top \quad \text{and} \quad \tilde{\theta}_s(t) = \delta \tanh\left(\frac{t-1/2}{\delta^2}\right). \quad (37)$$

Theorem 2.3 gives the requirement  $c_2(a, t) = 0$  and

$$\begin{aligned} c_1(a, t) = & \delta (2 - 2\pi^2 A t + \pi^2 A) \left[ \tanh\left(\frac{t-1/4}{\delta^2}\right) - \tanh\left(\frac{t-3/4}{\delta^2}\right) \right] \\ & + \frac{2t-1}{\delta} \left[ \operatorname{sech}^2\left(\frac{t-1/4}{\delta^2}\right) - \operatorname{sech}^2\left(\frac{t-3/4}{\delta^2}\right) \right], \end{aligned}$$

while applying the shear conditions of Theorem 2.2 as in the previous example locally near  $(1, 0)$  gives  $c_2(x, t) = 0$  and

$$c_1(x, t) = \left[ \delta 2\pi^2 A \tanh\left(\frac{t-1/2}{\delta^2}\right) - \frac{1}{\delta} \operatorname{sech}^2\left(\frac{t-1/2}{\delta^2}\right) \right] x_2 I_{(1,0)}(x_1, x_2).$$

Thus, a control velocity which simultaneously attempts to achieve the required hyperbolic trajectory and tangent vector rotation can be constructed by summing these:

$$\begin{pmatrix} c_1(x_1, x_2, t) \\ c_2(x_1, x_2, t) \end{pmatrix} = \delta \begin{pmatrix} (2 - 2\pi^2 A t + \pi^2 A) \left[ \tanh\left(\frac{t1/4}{\delta^2}\right) - \tanh\left(\frac{t3/4}{\delta^2}\right) \right] + 2\pi^2 A \tanh\left(\frac{t1/2}{\delta^2}\right) x_2 I_{(1,0)}(x_1, x_2) \\ 0 \end{pmatrix} + \frac{1}{\delta} \begin{pmatrix} (2t-1) \left[ \operatorname{sech}^2\left(\frac{t1/4}{\delta^2}\right) - \operatorname{sech}^2\left(\frac{t3/4}{\delta^2}\right) \right] - \operatorname{sech}^2\left(\frac{t1/2}{\delta^2}\right) x_2 I_{(1,0)}(x_1, x_2) \\ 0 \end{pmatrix}. \quad (38)$$

The  $1/\delta$  terms above represent the spikes (associated with the time-derivatives in (36)) needed; these are smoothed versions of Dirac impulses. The system (32) was numerically examined with  $c$  given by (38), with the choice of parameters  $A = 1$  and  $\delta = 0.1$ . The  $t$ -discretisation of the previous example was used, with the forward FTLE field computed at each time using the maximum available data (i.e., till  $T = 2$ ). By evaluating the slopes and intercepts from the extracted ridge, the values of  $\theta_s(t)$  and the  $x_1$ -component of  $a(t)$  were respectively computed at values of  $t \in [0, 1]$ . The results, in circles, are compared with the required curves (37) in Fig. 8. There is some error near the abrupt changes, which is inevitable since the FTLE ridges become ambiguous at discontinuities. Nevertheless, the efficacy of the control strategy in this nearly discontinuous situation is remarkable.

## 4 Concluding remarks

This article approaches the issue of nonautonomous eigenvector analogues, as time-varying local tangents to stable and unstable manifolds, from two perspectives. First, it hopes to address the finite-time situation in a sense that would appear reasonable with data availability, while retaining the nonautonomous viewpoint within this finite time-range. Under the ansatz of the flow being nearly autonomous, leading-order approximations for finite-time nonautonomous analogues to saddle fixed points and their eigenvectors were stated, building respectively on the infinite-time results of Theorems 2.1 and 2.2. The relationship between the eigenvector rotation to the nonautonomous

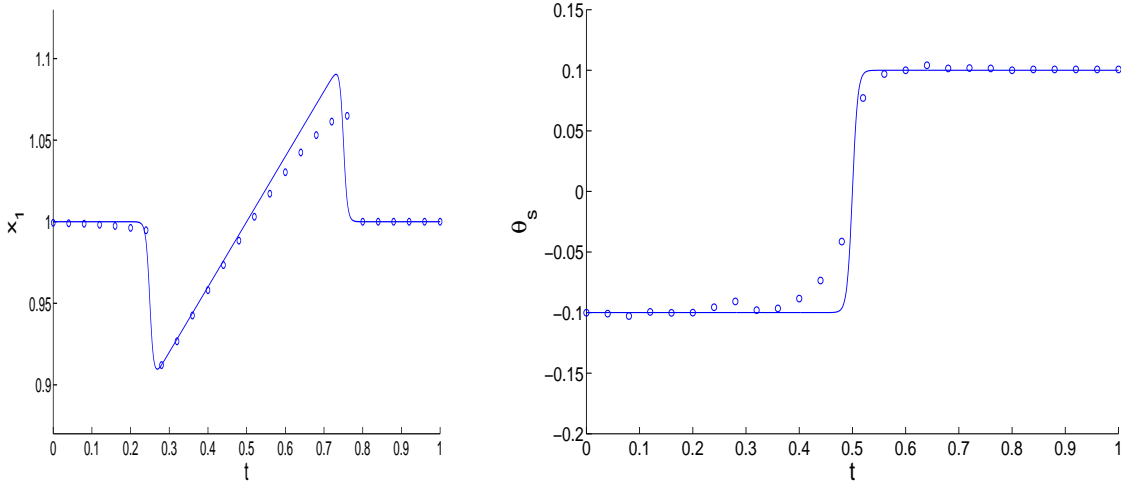


Figure 8: Results for the control velocity (38) with  $\delta = 0.1$ ,  $A = 1$ , and  $T = 2$ , extracted by computing the intercept and slope of the FTLE ridges using linear regression [circles]:  $x_1$ -coordinate of hyperbolic trajectory (left panel) and  $\theta_s$  (right panel) along with the required curves (37) [solid].

tangent vectors to the local invariant manifolds and the local nonautonomous velocity shear was quantified. An attempt to characterise how unknown data from outside the finite-time interval affects flow entities was introduced, by investigating the dependence of an error which depends on the finiteness parameter  $T$ . The nearly autonomous hypothesis is of course restrictive, and one potential extension would be to assume that the flow is a perturbation of a nearby flow which, while not necessarily autonomous, has its relevant features (hyperbolic trajectory, stable and unstable manifolds) *known*. This idea was formally used recently [14] for controlling high-dimensional hyperbolic trajectories.

Second, this article addresses the question of controlling the direction of emanation of stable and unstable manifolds from a hyperbolic trajectory, i.e., controlling analogues of eigenvectors. Such local results influence the *global* stable and unstable manifolds, i.e., the global transport templates, since exponential decay definitions [27, 16, 65] for global invariant manifolds depend on *local* decay; standard approaches for defining global stable and unstable manifolds [42, 3] indeed depend on first defining local stable/unstable manifolds, and then obtaining the global manifolds by ‘flowing’ these in time. The local shear velocity required for a given nonautonomous motion of these directions was obtained in Theorem 2.4. The finite-time version of these (see Remark 2.4) simply uses the full data available in the time-range  $[-T, T]$  in doing the computation of the shear requirement.

The efficacy of this finite-time process was numerically demonstrated using both a time-periodic and a time-discontinuous specification of the tangent vector directions, the latter situation pushing the boundaries of the theorems. To achieve genuinely time-discontinuous flow trajectories, impulsive terms are required in the velocities. It has been shown that in the presence of impulsive vector fields one needs to think of stable and unstable *pseudo*-manifolds which reset themselves at the time instance at which there is an impulse [5, 11]. For the purposes of the numerical verifications of this article, marginally smoothed versions of the discontinuous functions were employed. In both the time-periodic and time-impulsive implementations of the control strategy, excellent performance (as measured by the rotation of FTLE ridges with time) was obtained. Any specified (but small) time-varying reorientation of the stable and unstable manifold directions seems to be possible, providing a tool for controlling the essential skeleton of fluid flows. In particular, by focussing energy on a *localised* region near the time-varying hyperbolic trajectory, a global transport impact can be achieved. Further analysis and development of these idea, building also on [13, 14, 15], are underway.

## A Proof of Theorem 2.2 (‘Eigenvector directions’)

The system (1) is, under the conditions of Hypothesis 2.1, equivalent to

$$\dot{x} = f(x) + [F(x, t, \varepsilon) - F(x, t, 0)] =: f(x) + \varepsilon h(x, t) + \mathcal{O}(\varepsilon^2) \quad (39)$$

where the higher-order term is uniformly bounded, and  $g(x, t) = \varepsilon h(x, t) + \mathcal{O}(\varepsilon^2)$ . Let  $\bar{x}^s(p)$  be a solution to (39) when  $\varepsilon = 0$  such that  $\bar{x}^s(p) \rightarrow a$  as  $p \rightarrow \infty$ ; this solution can be used to parametrise a branch of  $a$ ’s stable manifold for  $p \in [P, \infty]$ , for  $P$  as negative as required. Now, Balasuriya [6, 8] shows that when  $\varepsilon \neq 0$ , the perturbed stable manifold can be parametrised by  $(p, t)$  in the form

$$x^s(p, t) = \bar{x}^s(p) + \varepsilon \left[ \frac{M^s(p, t)}{|f(\bar{x}^s(p))|^2} f^\perp(\bar{x}^s(p)) + \frac{B^s(p, t)}{|f(\bar{x}^s(p))|^2} f(\bar{x}^s(p)) \right] + \varepsilon^2 \tilde{E}^s(p, t, \varepsilon) \quad (40)$$

where  $p$  represents the position and  $t$  the time-slice, on the perturbed stable manifold, and  $\tilde{E}^s$  is characterised by the presence of  $\tilde{K}_s$  for  $(p, t) \in [P, \infty) \times [T_s, \infty)$  for arbitrarily negative  $P$  and  $T_s$  such that

$$\left| \tilde{E}^s(p, t, \varepsilon) \right| + \left| \frac{\partial \tilde{E}^s(p, t, \varepsilon)}{\partial p} \right| \leq \tilde{K}_s. \quad (41)$$

The quantities  $M^s$  and  $B^s$  are given by [6]

$$M^s(p, t) := - \int_t^\infty \exp \left[ \int_{\tau-t+p}^p \nabla \cdot f \left( \bar{x}^s(\xi) \right) d\xi \right] f^\perp \left( \bar{x}^s(\tau-t+p) \right) \cdot h \left( \bar{x}^s(\tau-t+p), \tau \right) d\tau \quad (42)$$

and

$$B^s(p, t) := |f \left( \bar{x}^s(p) \right)|^2 \int_{t-p}^t \frac{R^s(\tau-t+p)M^s(p, \tau) + f \left( \bar{x}^s(\tau-t+p) \right) \cdot h \left( \bar{x}^s(\tau-t+p), \tau \right)}{|f \left( \bar{x}^s(\tau-t+p) \right)|^2} d\tau \quad (43)$$

where

$$R^s(\xi) := \frac{f \left( \bar{x}^s(\xi) \right) \left[ Df \left( \bar{x}^s(\xi) \right) + (Df)^\top \left( \bar{x}^s(\xi) \right) \right] f^\perp \left( \bar{x}^s(\xi) \right)}{|f \left( \bar{x}^s(\xi) \right)|^2}.$$

The above are mildly different representations of the results of Balasuriya's Theorems 2.7 and 2.8 [6]. Now, as  $p \rightarrow \infty$ ,  $x^s(p, t) \rightarrow a(t)$ , the hyperbolic trajectory, along the stable manifold direction, in each fixed time-slice  $t$ . Thus, the tangent vector to this, at the point  $a(t)$ , can be obtained by applying the limit  $p \rightarrow \infty$  to the  $p$ -derivative of  $x^s(p, t)$ . This is

$$x_p^s = \bar{x}_p^s + \varepsilon \left[ \frac{M_p^s f_p^\perp}{|f|^2} + \left( \frac{M_p^s}{|f|^2} - \frac{2M^s f \cdot f_p}{|f|^2} \right) f^\perp \right] + \varepsilon \left[ \frac{B_p^s f_p + B_p^s f}{|f|^2} - \frac{2B^s (f \cdot f_p)}{|f|^2} f \right] + \varepsilon^2 \tilde{E}_p^s,$$

where the  $p$ -subscript represents the partial derivative, and the arguments  $(p, t)$  for  $M^s$  and  $B^s$ , and the argument  $\bar{x}^s(p)$  for  $f$  have been suppressed for brevity. Since the  $p \rightarrow \infty$  limit is required, in this limit

$$\bar{x}^s(p) \sim a + cv_s e^{\lambda_s p} \quad (44)$$

for a constant  $c \neq 0$  can be applied; this is since the linearised flow  $\dot{y} = (Df)y$  dominates near  $a$ , and  $\bar{x}^s$  specifically comes in along the stable manifold (tangential to  $v_s$  with decay rate  $\lambda_s$ ) in this limit. The  $c$  represents a choice of 'initial condition' along the stable manifold, and as will be clear, is inconsequential in the final result. Now,  $f \left( \bar{x}^s(p) \right) = \bar{x}_p^s(p)$  since  $\bar{x}^s(p)$  is a solution to (39) when  $\varepsilon = 0$ , and thus

$$f \left( \bar{x}^s(p) \right) \sim c\lambda_s v_s e^{\lambda_s p} \quad , \quad f^\perp \left( \bar{x}^s(p) \right) \sim c\lambda_s v_s^\perp e^{\lambda_s p} \quad \text{and} \quad f_p \left( \bar{x}^s(p) \right) \sim c\lambda_s^2 v_s e^{\lambda_s p}. \quad (45)$$

Substituting these large  $p$  values into the expression for  $x_p^s$  yields

$$x_p^s = c\lambda_s e^{\lambda_s p} v_s + \frac{\varepsilon}{c\lambda_s e^{\lambda_s p}} \left[ (M_p^s - \lambda_s M^s) v_s^\perp + (B_p^s - \lambda_s B^s) v_s \right] + \varepsilon^2 \tilde{E}_p^s.$$

The rotational angle  $\theta_s$  from  $v_s$  towards  $v_s^\perp$  is  $\mathcal{O}(\varepsilon)$  and thus equal to  $\tan \theta_s$  to leading-order. This is essentially the slope of the above tangent line in an axis system  $(v_s, v_s^\perp)$ . Thus

$$\theta_s = \frac{\varepsilon (M_p^s - \lambda_s M^s) + \mathcal{O}(\varepsilon^2)}{c\lambda_s e^{\lambda_s p} \left[ c\lambda_s e^{\lambda_s p} + \frac{\varepsilon (B_p^s - \lambda_s B^s)}{c\lambda_s e^{\lambda_s p}} + \mathcal{O}(\varepsilon^2) \right]} = \varepsilon \frac{M_p^s - \lambda_s M^s}{c^2 \lambda_s^2 e^{2\lambda_s p}} + \mathcal{O}(\varepsilon^2) \quad (46)$$

as  $p \rightarrow \infty$ . Noteworthy is the fact that the tangential component associated with  $B^s$  contributes only to higher-order. The  $p$ -derivative of (42) is now required in the limit  $p \rightarrow \infty$ . In this limit, as  $\bar{x}^s$  approaches  $a$ ,  $\nabla \cdot f(\bar{x}^s(p)) \rightarrow \lambda_s + \lambda_u$  since the trace of  $Df$  at  $a$  is the sum of its eigenvalues. Putting this along with the other large  $p$  estimates in (45) into (42) gives the large  $p$  estimate

$$M^s(p, t) = -c\lambda_s e^{\lambda_u t} e^{\lambda_s p} \int_t^\infty e^{\lambda_u \tau} h^\perp \left( a + cv_s e^{\lambda_s(\tau-t+p)}, \tau \right) d\tau.$$

When computing  $M_p^s - \lambda_s M^s$ , the fact that  $M^s$  is a product of  $e^{\lambda_s p}$  with another function of  $p$  leads to cancellations, and results in

$$\begin{aligned} M_p^s - \lambda_s M^s &= -c\lambda_s e^{\lambda_u t} e^{\lambda_s p} \int_t^\infty e^{-\lambda_u \tau} \nabla h^\perp \left( a + cv_s e^{\lambda_s(\tau-t+p)}, \tau \right) \cdot \left( c\lambda_s v_s e^{\lambda_s(\tau-t+p)} \right) d\tau \\ &= -c^2 \lambda_s^2 e^{(\lambda_u - \lambda_s)t} e^{2\lambda_s p} \int_t^\infty e^{(\lambda_s - \lambda_u)\tau} v_s \cdot \nabla h^\perp \left( a + cv_s e^{\lambda_s(\tau-t+p)}, \tau \right) d\tau. \end{aligned}$$

Substituting into (46), putting in  $g = \varepsilon h + \mathcal{O}(\varepsilon^2)$ , and applying  $p \rightarrow \infty$  gives (12), where the  $\mathcal{O}(\varepsilon^2)$  terms have been combined into one term  $\varepsilon^2 E_s(t, \varepsilon)$  with bounded  $E_s(t, \varepsilon)$  for  $t \in [T_s, \infty)$ . The fact that the  $t$ -derivative of  $E_s$  is also bounded arises from the process of taking the  $t$ -derivative of (46) and utilising the fact that  $F \in C_{\text{unif}}^2(\Omega \times \mathbb{R} \times [0, \varepsilon_0))$  as specified in Hypothesis 2.1; this ensures the ability to take the  $t$ -derivative of the error terms in (46) and allow the terms multiplying  $\varepsilon^2$  to remain bounded.

Now, (13) is similarly derived, by using the unstable manifold formulation (Theorems 2.1 and 2.3) due to Balasuriya [6]. The expressions (40) and (42) change slightly, but there is no substantive difference in the derivation strategy, which shall be skipped for brevity.  $\square$

**Acknowledgements:** Support from Australian Research Council grant FT130100484, and conversations with Gary Froyland, are gratefully acknowledged.

## References

- [1] M. Allshouse and T. Peacock. refining finite-time Lyapunov ridges and the challenges of classifying them. *Chaos*, 25:987410, 2015.
- [2] M. Allshouse and J.-L. Thiffeault. Detecting coherent structures using braids. *Phys. D.*, 241:95–105, 2012.
- [3] D.K. Arrowsmith and C.M. Place. *An Introduction to Dynamical Systems*. University of Cambridge Press, Cambridge, 1990.

- [4] S. Balasuriya. Direct chaotic flux quantification in perturbed planar flows: general time-periodicity. *SIAM J. Appl. Dyn. Sys.*, 4:282–311, 2005.
- [5] S. Balasuriya. Cross-separatrix flux in time-aperiodic and time-impulsive flows. *Nonlinearity*, 19:2775–2795, 2006.
- [6] S. Balasuriya. A tangential displacement theory for locating perturbed saddles and their manifolds. *SIAM J. Appl. Dyn. Sys.*, 10:1100–1126, 2011.
- [7] S. Balasuriya. Explicit invariant manifolds and specialised trajectories in a class of unsteady flows. *Phys. Fluids*, 24:12710, 2012.
- [8] S. Balasuriya. Nonautonomous flows as open dynamical systems: characterising escape rates and time-varying boundaries. In W. Bahsoun, G. Froyland, and C. Bose, editors, *Ergodic Theory, Open Dynamics and Coherent Structures*, volume 70 of *Springer Proceedings in Mathematics and Statistics*, chapter 1, pages 1–30. Springer, 2014.
- [9] S. Balasuriya. Dynamical systems techniques for enhancing microfluidic mixing. *J. Micromech. Microeng.*, page in press, 2015.
- [10] S. Balasuriya. Quantifying transport within a two-cell microdroplet induced by circular and sharp channel bends. *Phys. Fluids*, 27:052005, 2015.
- [11] S. Balasuriya. Impulsive perturbations to differential equations: stable/unstable pseudo-manifolds, heteroclinic connections, and flux. page submitted, 2016.
- [12] S. Balasuriya, G. Froyland, and N. Santitissadeekorn. Absolute flux optimising curves of flows on a surface. *J. Math. Anal. Appl.*, 409:119–139, 2014.
- [13] S. Balasuriya and K. Padberg-Gehle. Controlling the unsteady analogue of saddle stagnation points. *SIAM J. Appl. Math.*, 73:1038–1057, 2013.
- [14] S. Balasuriya and K. Padberg-Gehle. Accurate control of hyperbolic trajectories in any dimension. *Phys. Rev. E*, 90:032903, 2014.
- [15] S. Balasuriya and K. Padberg-Gehle. Nonautonomous control of stable and unstable manifolds in two-dimensional flows. *Phys. D*, 276:48–60, 2014.

- [16] F. Battelli and C. Lazzari. Exponential dichotomies, heteroclinic orbits and Melnikov functions. *J. Differential Equations*, 86:342–366, 1990.
- [17] A. Berger, T. Doan, and S. Siegmund. A definition of spectrum for differential equations on finite time. *J. Differential Equations*, 246:1098–1118, 2009.
- [18] D. Blazeovski and R. de la Llave. Time-dependent scattering theory for ODEs and applications to reaction dynamics. *J. Phys. A: Math. Theor.*, 44:195101, 2011.
- [19] D. Blazeovski and J. Franklin. Using scattering theory to compute invariant manifolds and numerical results for the laser-driven Hénon-Heiles system. *Chaos*, 22:043138, 2012.
- [20] D. Blazeovski and G. Haller. Hyperbolic and elliptic transport barriers in three-dimensional unsteady flows. *Phys. D*, 273:46–62, 2014.
- [21] M. Branicki and S. Wiggins. An adaptive method for computing invariant manifolds in non-autonomous, three-dimensional dynamical systems. *Phys. D*, 238:1625–1657, 2009.
- [22] M. Branicki and S. Wiggins. Finite-time Lagrangian transport analysis: stable and unstable manifolds of hyperbolic trajectories and finite-time Lyapunov exponents. *Nonlin. Proc. Geophys.*, 17:1–36, 2010.
- [23] M. Budišić and I. Mezić. Geometry of ergodic quotient reveals coherent structures in flows. *Phys. D*, 241:1255–1269, 2012.
- [24] M. Budišić and J.-L. Thiffeault. Finite-time braiding exponents. *Chaos*, 25:087407, 2015.
- [25] S. Chandrasekhar. *Hydrodynamics and Hydrodynamic Stability*. Dover, New York, 1961.
- [26] A. Chian, E. Rempel, G. Aulanier, B. Schmeister, S. Shadden, B. Welsch, and A. Yeates. Detection of coherent structures in turbulent photospheric flows. *Astrophys. J.*, 786:51, 2014.
- [27] W. A. Coppel. *Dichotomies in Stability Theory*. Number 629 in Lecture Notes Math. Springer-Verlag, Berlin, 1978.
- [28] T. Doan, D. Karrasch, N. Yet, and S. Siegmund. A unified approach to finite-time hyperbolicity which extends finite-time Lyapunov exponents. *J. Differential Equations*, 252:5535–5554, 2012.



- [29] F. d’Ovidio, V. Fernández, E. Hernández-García, and C. López. Mixing structure in the Mediterranean sea from finite-size Lyapunov exponents. *Geophys. Res. Lett.*, 31:L17203, 2004.
- [30] L. Duc and S. Siegmund. Existence of finite-time hyperbolic trajectories for planar Hamiltonian flows. *J. Dyn. Differential Equations*, 23:475–494, 2011.
- [31] M. Farazmand and G. Haller. Attracting and repelling Lagrangian coherent structures from a single computation. *Chaos*, 15:023101, 2013.
- [32] A. Fortin, T. Briffard, and A. Garon. A more efficient anisotropic mesh adaptation for the computation of Lagrangian Coherent Structures. *J. Computational Phys.*, 285:100–110, 2015.
- [33] G. Froyland. An analytic framework for identifying finite-time coherent sets in time-dependent dynamical systems. *Phys. D*, 250:1–19, 2013.
- [34] G. Froyland, S. Lloyd, and A. Quas. Coherent structures and isolated spectrum for Perron–Frobenius cocycles. *Ergod. Th. & Dynam. Sys.*, 30:729–756, 2010.
- [35] G. Froyland and K. Padberg. Almost invariant sets and invariant manifolds: connecting probabilistic and geometric descriptions of coherent structures in flows. *Phys. D*, 238:1507–1523, 2009.
- [36] G. Froyland and K. Padberg-Gehle. Almost-invariant and finite-time coherent sets: directionality, duration, and diffusion. In W. Bahsoun, C. Bose, and G. Froyland, editors, *Ergodic Theory, Open Dynamics, and Coherent Structures*, pages 171–216. Springer, 2014.
- [37] G. Froyland, N. Santitissadeekorn, and A. Monahan. Transport in time-dependent dynamical systems: Finite-time coherent sets. *Chaos*, 20:043116, 2010.
- [38] L. Gaultier, B. Djath, J. Verron, J.-M. Brankart, P. Brasseur, and A. Melet. Inversion of submesoscale patterns from a high-resolution Solomon Sea model: feasibility assessment. *J. Geophys. Res. Oceans*, 119:4520–4541, 2014.
- [39] F. Ginelli, H. Chaté, R. Livi, and A. Politi. Covariant Lyapunov vectors. *J. Phys. A: Math. Theor.*, 46:254005, 2013.

- [40] M. Green, C. Rowley, and A. Smits. The unsteady three-dimensional wake produced by a trapezoidal panel. *J. Fluid Mech.*, 685:117–145, 2011.
- [41] J. Guckenheimer. From data to dynamical systems. *Nonlinearity*, 27:R41–R50, 2014.
- [42] J. Guckenheimer and P. Holmes. *Nonlinear Oscillations, Dynamical Systems and Bifurcations of Vector Fields*. Springer, New York, 1983.
- [43] J. Hale. Integral manifolds of perturbed differential systems. *Annals Math.*, 73:496–531, 1961.
- [44] G. Haller. A variational theory for Lagrangian coherent structures. *Phys. D*, 240:574–598, 2011.
- [45] G. Haller. Lagrangian Coherent Structures. *Annu. Rev. Fluid Mech.*, 47:137–162, 2015.
- [46] G. Haller and F. Beron-Vera. Geodesic theory for transport barriers in two-dimensional flows. *Phys. D*, 241:1680–1702, 2012.
- [47] G. Haller and A.C. Poje. Finite time transport in aperiodic flows. *Phys. D*, 119:352–380, 1998.
- [48] G. Haller and G.-C. Yuan. Lagrangian coherent structures and mixing in two-dimensional turbulence. *Phys. D*, 147:352–370, 2000.
- [49] D. Karrasch. Linearization of hyperbolic finite-time processes. *J. Differential Equations*, 254:254–282, 2013.
- [50] D. Karrasch, M. Farazmand, and G. Haller. Attraction-based computation of hyperbolic Lagrangian Coherent Structures. *J. Computational Dyn.*, 2:83–93, 2015.
- [51] D. Karrasch and G. Haller. Do Finite-Size Lyapunov Exponents detect coherent structures? *Chaos*, 23:043126, 2013.
- [52] D. Kelley, M. Allshouse, and N. Ouellette. Lagrangian coherent structures separate dynamically distinct regions in fluid flow. *Phys. Rev. E*, 88:013017, 2013.
- [53] J. Lamb, M. Rasmussen, and C. Rodrigues. Topological bifurcations of minimal invariant sets for set-valued dynamical systems. *Proc. Amer. Math. Soc.*, page in press, 2015.

- [54] C. Liang, G. Liao, and W. Sun. A note on approximating properties of the Oseledets splitting. *Proc. Amer. Math. Soc.*, 142:3825–3838, 2014.
- [55] T. Ma and E. Bollt. Differential geometry perspective of shape coherence and curvature evolution by finite-time nonhyperbolic splitting. *SIAM J. Appl. Dyn. Sys.*, 13:1106–1136, 2014.
- [56] A.M. Mancho, D. Small, S. Wiggins, and K. Ide. Computation of stable and unstable manifolds of hyperbolic trajectories in two-dimensional, aperiodically time-dependent vector fields. *Phys. D*, 182:188–222, 2003.
- [57] A.M. Mancho, S. Wiggins, J. Curbelo, and C. Mendoza. Lagrangian descriptors: A method for revealing phase space structures of general time dependent dynamical systems. *Commun. Nonlin. Sci. Numer. Simu.*, 18:3530–3557, 2013.
- [58] I. Mezić, S. Loire, V. Fonoberov, and P. Hogan. A new mixing diagnostic and Gulf oil spill movement. *Science*, 330:486–489, 2010.
- [59] P.D. Miller, C.K.R.T. Jones, A.M. Rogerson, and L.J. Pratt. Quantifying transport in numerically generated velocity fields. *Phys. D*, 110:105–122, 1997.
- [60] B.A. Mosovsky and J.D. Meiss. Transport in transitory dynamical systems. *SIAM J. Appl. Dyn. Sys.*, 10:35–65, 2011.
- [61] D. Nelson and G. Jacobs. DG-FTLE:Lagrangian Coherent Structures with high-order discontinuous Galerkin methods. *J. Computational Phys.*, 295:65–86, 2015.
- [62] K.-D. Nguyen Thu Lam and J. Kurchan. Stochastic perturbation of integrable systems: A window to weakly chaotic systems. *J. Stat. Phys.*, 156:619–646, 2014.
- [63] G. Norgard and P.-T. Bremer. Second derivative ridges are straight lines and the implications for computing Lagrangian coherent structures. *Phys. D*, 241:1475–1476, 2012.
- [64] V. Oseledets. Multiplicative ergodic theorem: Characteristic Lyapunov exponents of dynamical systems. *Trudy MMO*, 19:179–210, 1968.

- [65] K.J. Palmer. Exponential dichotomies and transversal homoclinic points. *J. Differ. Equations*, 55:225–256, 1984.
- [66] T. Peacock and J. Dabiri. Introduction to focus issue: Lagrangian Coherent Structures. *Chaos*, 20:017501, 2010.
- [67] T. Peacock and G. Haller. Lagrangian coherent structures: the hidden skeleton of fluid flow. *Phys. Today*, 66:41–47, 2013.
- [68] A. Poje, G. Haller, and I. Mezić. The geometry and statistics of mixing in aperiodic flows. *Phys. Fluids*, 11:2963–2968, 1999.
- [69] B. Sandstede, S. Balasuriya, C.K.R.T. Jones, and P.D. Miller. Melnikov theory for finite-time vector fields. *Nonlinearity*, 13:1357–1377, 2000.
- [70] B. Schindler, R. Peikert, R. Fuchs, and H. Theisl. Ridge concepts for the visualization of Lagrangian coherent structures. In R. Peikert, H. Hauser, H. Carr, and R. Fuchs, editors, *Topological methods in data analysis and visualization II*, pages 221–236. Springer, 2012.
- [71] S.C. Shadden, F. Lekien, and J.E. Marsden. Definition and properties of Lagrangian coherent structures from finite-time Lyapunov exponents in two-dimensional aperiodic flows. *Phys. D*, 212:271–304, 2005.
- [72] A. Stroock, S. Dertinger, A. Adjari, I. Mezić, H. Stone, and G. Whitesides. Chaotic mixer for microchannels. *Science*, 295:647–651, 2002.
- [73] G. Taylor and A. Green. Mechanism for the production of small eddies from larger ones. *Proc. R. Soc. Lond. A*, 158:499–521, 1937.
- [74] H. Teramoto, G. Haller, and T. Komatsuzaki. Detecting invariant manifolds as stationary LCSs in autonomous dynamical systems. *Chaos*, 23:043107, 2013.
- [75] G. Wang, F. Yang, and W. Zhao. There can be turbulence in microfluidics at low Reynolds number. *Lab Chip*, 14:1452–1458, 2014.
- [76] G. Whitesides. The origins and the future of microfluidics. *Nature*, 442:368–373, 2006.

- [77] K. Yagasaki. Invariant manifolds and control of hyperbolic trajectories on infinite- or finite-time intervals. *Dynamical Systems*, 23:309–331, 2008.
- [78] Y. Yi. A generalized integral manifold theorem. *J. Differential Equations*, 102:153–187, 1993.
- [79] Y. Yi. Stability of integral manifold and orbital attraction of quasi-periodic motion. *J. Differential Equations*, 103:278–322, 1993.